THE POSSIBLE ROLE OF SYMMETRIC INSTABILITY IN THE FORMATION OF PRECIPITATION BANDS

by

MARC ALLEN SELTZER

B.S., McGill University

(1982)

SUBMITTED TO THE DEPARTMENT OF

EARTH, ATMOSPHERIC AND PLANETARY SCIENCES

IN PARTIAL FULFILLMENT OF THE

REQUIREMENTS FOR THE DEGREE OF

MASTER OF SCIENCE

at the

MASSACHUSETTS INSTITUTE OF TECHNOLOGY

May 1984

Signature of Author _____
Department of Earth, Atmospheric and Planetary Sciences
May 1984

Certified by _____
Richard E. Passarelli
Thesis Supervisor

Accepted by _____
Theodore R. Madden
Chairman, Departmental Committee on Graduate Students

THE POSSIBLE ROLE OF SYMMETRIC INSTABILITY IN THE FORMATION OF PRECIPITATION BANDS

by

MARC ALLEN SELTZER

Submitted to the Department of
Earth, Atmospheric and Planetary Sciences
in partial fulfillment of the requirements for the degree of
Master of Science in Meteorology

ABSTRACT

Fifteen cases of banded and non-banded precipitation that are not associated with any surface frontal regions are presented. An attempt is made to relate the atmospheric conditions associated with the banded observations to the theory of symmetric instability. Linear perturbation theory and parcel theory are used to assess this instability and to make predictions of the strength and orientation of the observed bands. The theory does explain many of the banded features considered in this study: all of the bands are aligned parallel to the thermal wind; strong shear and near-neutral static stabilities are observed when bands occur; multiple bands have a wavelength that is related to the depth of the unstable region and the slope of isentropic surfaces. The theory, however, does not fully explain the propagation of some bands relative to the mean flow. Furthermore, symmetric instability is an imbalance that can arise in a geostrophically balanced atmosphere. The observations indicate that in some cases, the flow is not in geostrophic balance. Most of the indications of symmetric instability are due to narrow shear regions that do not seem to be in geostrophic balance.

Thesis Supervisor: Dr. Richard E. Passarelli

Title: Professor of Meteorology

1. Introduction.

"It is now well established that the regions of heaviest precipitation in extratropical cyclones are often organized on the mesoscale in the form of rainbands." (Parsons and Hobbs, 1983). Some of these bands are directly associated with frontal circulations. Others occur far from any regions of frontal forcing. While much is known about mesoscale bands caused by frontogenesis alone, little is known about those bands that occur far from the region of frontal forcing. In this thesis, the possible role of symmetric instability in the formation of these precipitation bands is examined.

The data set used in this study comes from the M.I.T. NEWS (New England Winter Storms) Project. During three winters, 1981 to 1983, observations were taken from 20 storms with a Doppler radar, an aircraft, and standard National Weather Service data. In many of these storms intense precipitation bands occurred that were clearly not frontal in nature. These bands were usually embedded in regions of very strong shear and near neutral static stability.

This paper will attempt to answer three questions:

1. How do the observed atmospheric conditions during these storms compare to those assumed in theoretical models of symmetric instability?

2. Do the observed precipitation bands exhibit those features predicted by the theory of symmetric instability?

3. Using simple linear theory, how well can one predict the occurrence of these bands, and in so doing, say something about their strength and orientation?

It was Hoskins (1974) who perhaps first suggested that precipitation bands may be caused by symmetric instability. Many of the qualitative properties of symmetric instability in a dry inviscid atmosphere have been summarized by Bennetts and Hoskins (1979; hereafter referred to as BH). BH noticed that the observations of banded precipitation oriented along the vertical shear direction (see for example, Elliott and Hovind 1964; Browning and Harrold, 1969; Houze et al. 1976) fit well with the predictions of the classical theory of symmetric baroclinic instability developed by Solberg (1936), Eliassen (1962) and Ooyama (1966) among others. This theory, derived for a two dimensional situation, predicts an instability that produces roll circulations oriented along the shear of the geostrophic wind. While the effects of moisture are not considered in the original theory, BH proposed that the presence of moisture can lead to the observed banded convection. In this section the criterion for symmetric instability for the dry inviscid case will be reviewed

following BH. The extension of these results to include viscosity and moisture following the work of Emanuel (1979 and 1983) will then be discussed.

Symmetric instability is a type of instability that can occur in a geostrophically balanced atmosphere. It arises from an imbalance of the pressure gradient, Coriolis and buoyancy forces. Two different approaches can be taken to assess this instability. One approach is to examine the stability of a geostrophic basic state to infinitesimal perturbations. Normal mode solutions of the linearized equations of motion are sought and the maximum growth rate of the perturbation is determined. The second approach is to consider the finite displacement of an air parcel from its initial equilibrium state. This is analogous to the parcel method for assessing convective instability.

In the stability analyses reviewed in this section, four further assumptions are made:

1. The flow is inviscid and Boussinesq, and takes place on an f plane.

2. The basic state flow is in the y direction and is in geostrophic balance.

3. The basic state and perturbations vary only in the x and z directions.

4. The flow has constant horizontal and vertical shears.

Let $V(x,z)$ and $\theta(x,z)$ denote the basic state velocity and potential temperature fields. Geostrophic balance imp-

lies that V is related to θ by the thermal wind relation

$$f \frac{\partial V}{\partial z} = \frac{g}{\bar{\theta}} \frac{\partial \theta}{\partial x} \quad . \qquad (1.1)$$

Stone (1966) showed that for V varying linearly only in height, infinitesimal perturbations from this baroclinic basic state are unstable if the Richardson number Ri is less than unity, where

$$Ri = \frac{\frac{g}{\bar{\theta}} \frac{\partial \theta}{\partial z}}{\left(\frac{\partial V}{\partial z}\right)^2} \quad . \qquad (1.2)$$

BH extended Stone's analysis by allowing the basic state velocity V to have constant shear in both the x and z directions. This introduced a minor modification to the stability criterion. The flow is found to be unstable when

$$(\eta/f) \cdot Ri < 1 \qquad (1.3)$$

where $\eta = f + \partial V/\partial x$ is the absolute vorticity of the basic state flow. This instability condition is equivalent to the presence of negative absolute vorticity on isentropic surfaces. The orientation of the most unstable perturbation was shown to lie roughly halfway between the absolute vorticity vector and the isentropes.

BH also showed that for a saturated atmosphere, the effect of latent heat can be included in the stability criterion by replacing θ by θ_e, the equivalent potential temperature. In general it is found that the stability of the flow is decreased when the effects of moisture are included.

The inviscid analyses of symmetric instability by Stone and BH both conclude that the most unstable disturbance has an infinite wavenumber. In inviscid theory, there is no shortwave cutoff. Indeed, Emanuel (1979) showed that the addition of viscosity leads to a mesoscale wavelength for the most unstable disturbance. He showed that the unstable circulation has the following properties:

1. Streamlines (in the x-z plane) take the form of closed vortices elongated along isentropic surfaces.
2. The horizontal wavelength of the disturbance does not depend on viscosity except in the limit of weak diffusion.
3. The wavelength of the disturbance is such that the sloping vortices do not overlap in the horizontal direction. The wavelength is determined by the depth of the unstable layer and the slope of the isentropic surfaces.

Emanuel (1983) looked at the stability of the geostrophic basic state to finite parcel displacements. He assumed that V varies linearly and only in height. With this choice it can easily be shown that the quantity M which is equal to fx+V is conserved. A parcel displaced from its equilibrium position, will thus conserve both its original M and θ values. Accelerations for a displaced parcel (or more precisely a tube extending infinitely in the y direction) in the x and z directions are

$$\frac{du}{dt} = f(V_p - V_g) = f(M_p - M_g); \qquad (1.4)$$

$$\frac{dw}{dt} = \frac{g}{\bar{\theta}_g}(\theta_p - \theta_g) \qquad (1.5)$$

where the subscript g refers to the geostrophically balanced basic state and the subscript p refers to the parcel's value. Displaced parcels can accelerate both vertically and horizontally due to the surplus (or deficit) of the parcel's M and θ with respect to the environment.

Fig. 1 illustrates the stability characteristics for parcels displaced in the x-z plane. A possible basic state configuration of M and θ surfaces is indicated. M is chosen to increase upwards and to the right. θ is chosen to increase upward (a stable stratification).

Eqs. 1.4 and 1.5 can be used independently to determine the inertial and gravitational stability of a displaced parcel from the basic state, with horizontal displacements used to the assess inertial stability, and vertical displacements used to assess gravitational instability. The assessment of symmetric instability is made by imagining the displacements of parcels slantwise in the x-z plane and evaluating the accelerations of the parcel using both Eqs. 1.4 and 1.5.

For the basic state shown in Fig. 1, it is found that parcels displaced vertically or horizontally are stable (see for example points A and B). The parcel's resultant acceleration is back toward the parcel's origin. For slantwise displacements, however, it is found that if the

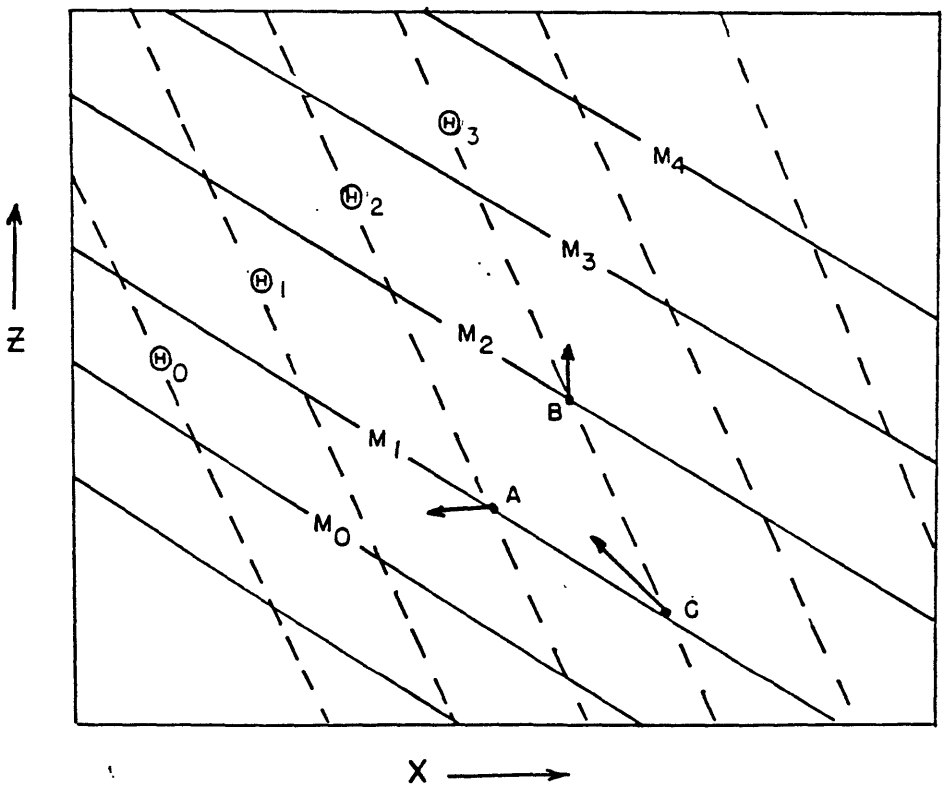

Fig. 1. Schematic vertical cross-section illustrating the use of the parcel technique in assessing symmetric instability. A possible basic state configuration of M and θ surfaces is indicated.

displacement has a slope that is greater than that of M surfaces but less than that of θ surfaces, the resultant acceleration will be in the direction of the displacement (see point C). The result of such a stability analysis reveals that symmetric instability will be possible only when M surfaces are more shallow than θ surfaces. It should be noted that for a saturated atmosphere, to a good approximation, the stability can be assessed in the same way by replacing θ by θ_e.

This parcel technique can also be applied to a single sounding. Emanuel (1983) has shown that for θ and V varying linearly in x and z, the stability of a slantwise displaced parcel can be evaluated by adding the value

$$\frac{1}{2}\frac{T_{vp}}{g}\frac{f}{\eta}\frac{\partial}{\partial z}\left\{(V-V_p)^2\right\}$$

to the reversibly lifted parcel temperature calculated in the usual way on a thermodynamic diagram. Tv is the virtual temperature. Parcels can then be lifted from different heights in a manner analogous to that of assessing ordinary (buoyant) convection. The level and orientation of the most unstable parcels for finite lifting can be determined by varying both the initial height and orientation of the parcel (or tube).

The nature of the circulations predicted by the linear theory of symmetric instability suggest that symmetric

instability might explain banded precipitation. Figure 2 (reproduced from Emanuel, 1979) shows the stream function associated with the onset of symmetric instability. Recall that the closed vortices in the x-z plane extend infinitely in the y direction. In the presence of moisture, precipitation is likely to form in the ascending branches of the circulation. The pattern of precipitation, when viewed at constant altitude with a radar, would take the form of a band oriented in the y direction (along the shear). In this respect, linear theory can explain the occurrence of precipitation bands.

Further support of this explanation must come from a comparison between the observations of atmospheric conditions in the vicinity of banded precipitation and the linear theory. For example, there are several observational checks that can be made:

1. The atmospheric conditions should be two dimensional with most of the variations in thermodynamic and kinematic properties occurring in the cross-band direction and in the vertical.
2. There should be a region in the atmosphere where the Richardson number instability criterion (e.g. Eq. 1.3) is met.
3. The bands should be aligned along the thermal wind and should be strongest in the region of instability.

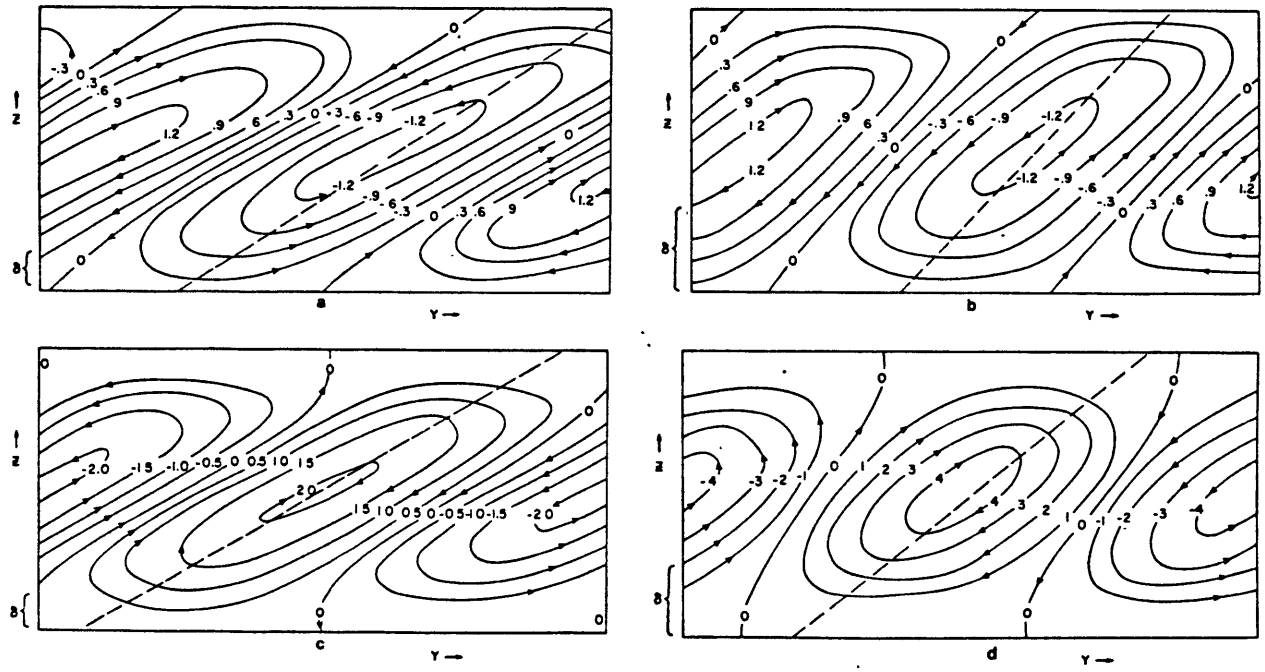

Fig. 2. Streamfunction associated with the onset of symmetric instability (reproduced from Emanuel, 1979). Plots (a) and (b) are solutions for free-slip boundaries with diffusion coefficient $T=10^{-4}$ and 1.6×10^{-3}, respectively. Plots (c) and (d) are solutions for no-slip boundaries with $T=10^{-4}$ and 10^{-3} respectively. The abscissa spans one full wavelength. The dashed line indicates the relative orientation of the potential isentropes.

4. If the bands are observed to be moving in the cross-band direction, they should be moving approximately with the mean flow in this direction. Note that the results of the present linear theory imply that the circulation pattern does not propagate relative to the basic-state flow in x.

5. Spacing between bands should be related to the depth of the unstable layer and the slope of isentropic surfaces.

6. The circulation pattern near the bands should include a region of ascending motion sloping nearly along isentropic surfaces.

2. Observations

The measurements of thermodynamic and kinematic properties were all taken from sounding data. Standard National Weather Service balloon soundings from Chatham, Massachusetts, Portland, Maine and Albany, New York, launched at nominal times as well as special launch times were used. Rawinsondes were also launched from M.I.T. In addition, aircraft measurements made by the NOAA P-3 were taken in a sounding mode at locations chosen to best supplement the other soundings. Data from mandatory and significant levels of the NWS soundings were used. All sounding data were interpolated to a 250-meter vertical grid.

The cases presented in this study were chosen to meet three requirements.

1. The low pressure center, as determined from surface analyses, was not near the region in question. This requirement excluded regions that had a generally more complicated mesoscale structure involving frontal zones and strongly curved flow.
2. Precipitation was observed on the M.I.T. radar.
3. Surface fronts were not present in the region.

Table 1 lists the fifteen cases that will be considered in this study.

A measure of bandedness of the precipitation was determined for each case. This was done subjectively by a group of four scientists from radar reflectivity patterns

Table 1.

Case	Banded-ness	B.O.	LMSW	FFS	DDS	Nd^2	Nw^2	850-500mb FFS
12/05/81	3	45	4.75	13.5	37	1.4	.8	8.0
12/06/81	3	0	2.75	13.3	5	1.6	1.2	8.3
12/16/81	3	45	1.75	18.6	39	2.0	1.1	7.1
12/11/82	1	70	4.00	11.2	55	6.9	4.0	5.2
12/12/82	2	50	3.75	17.1	51	2.3	1.7	14.6
12/20/82	2	0	2.00	14.5	-2	0.7	-3.8	5.1
01/11/83	3	0	3.00	19.4	14	2.5	2.5	4.3
01/24/83	0	-	4.25	8.2	129	1.5	0.6	5.0
02/03/83	0	-	3.25	7.9	90	2.4	2.1	5.8
02/12/83	3	80	5.50	13.4	66	1.8	1.4	9.5
11/28/83	3	135	2.75	21.2	117	3.0	4.3	5.0
12/03/83	1	90	5.75	11.5	115	.8	.4	6.0
12/04/83	0	-	5.25	22.4	63	2.2	1.8	5.7
12/06/83	0	-	2.00	9.6	120	3.8	-0.4	5.8
01/11/84	2	45	3.75	19.5	34	3.4	3.5	8.5

LMSW - level of maximum wind shear magnitude [km]
B.O. - band orientation [deg]
FFS - wind shear magnitude [m/s/km]
DDS : wind shear direction [deg]
Nd^2 : Brunt Vaiscala frequency (dry) [$10^{-4}sec^{-2}$]
Nw^2 : Brunt-Vaiscala frequency (moist) [$10^{-4}sec^{-2}$]

Note: FFS, DDS, Nd^2, Nw^2, computed at LMWS

such as that shown in Fig. 3. The criteria used to define bandedness were:

1. The elongation of the reflectivity distribution in the horizontal
2. The strength of the reflectivity factor anomaly, and
3. The band's temporal and spatial coherence.

A four-point scale was used, with 0 signifying non-banded and 3 meaning strongly banded.

2.1 The synoptic situation in a representative case

The cases classified as banded have some common synoptic-scale features. These features can be summarized by looking at one representative case. Fig. 4 shows the surface analysis for 00GMT on 6 December 1981. The low-pressure center is well to the east of Boston and any obvious surface fronts are far from the New England area. Figure 5 shows the 500-mb geopotential height and temperature field for the same time. Note the strong horizontal temperature gradients corresponding to large geostrophic wind shears in the New England area.

The corresponding radar reflectivity pattern was shown previously in Fig. 3. This constant-altitude presentation represents the average reflectivity factor in a layer from 2.5 to 4.0 km altitude. The dominant feature is a large band of very heavy precipitation oriented north-south. This

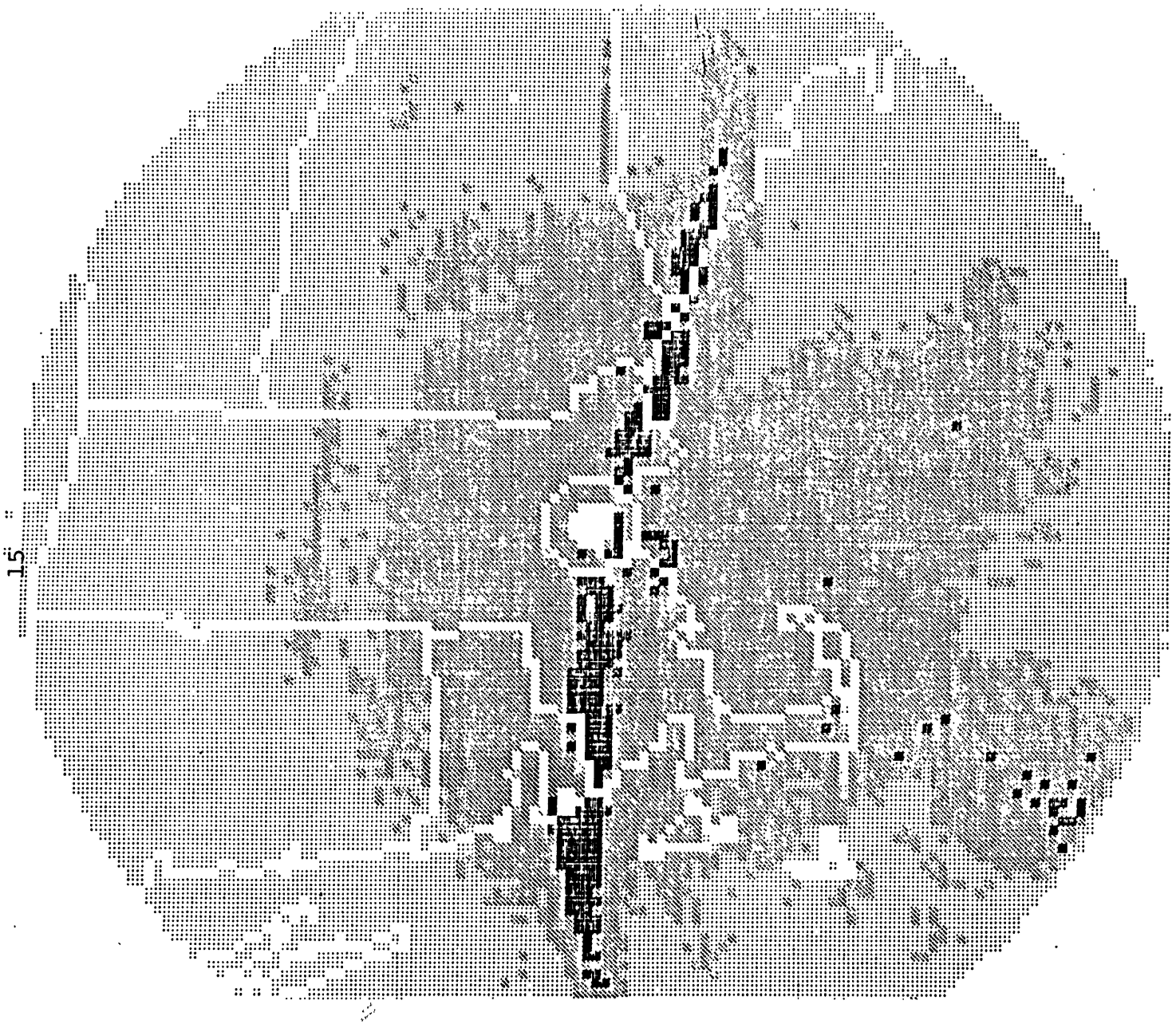

Fig. 3. Constant altitude planned position indicator showing the average reflectivity factor in a layer from 2.5 to 4.0 km altitude for 00GMT on 6 December 1981.

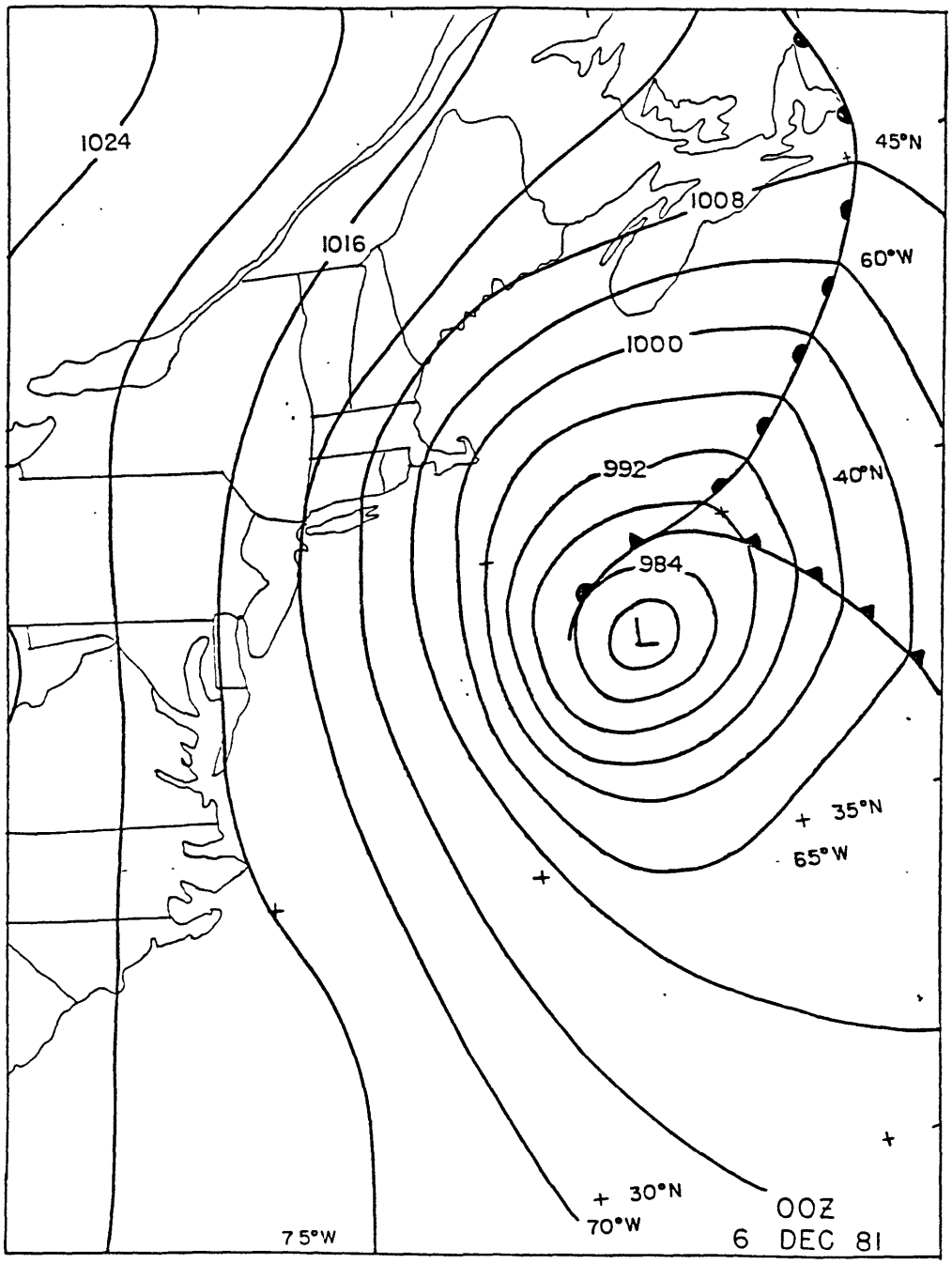

Fig. 4. Surface analysis for 00GMT on 6 December 1981, adapted from National Meteorological Center (NMC) analysis.

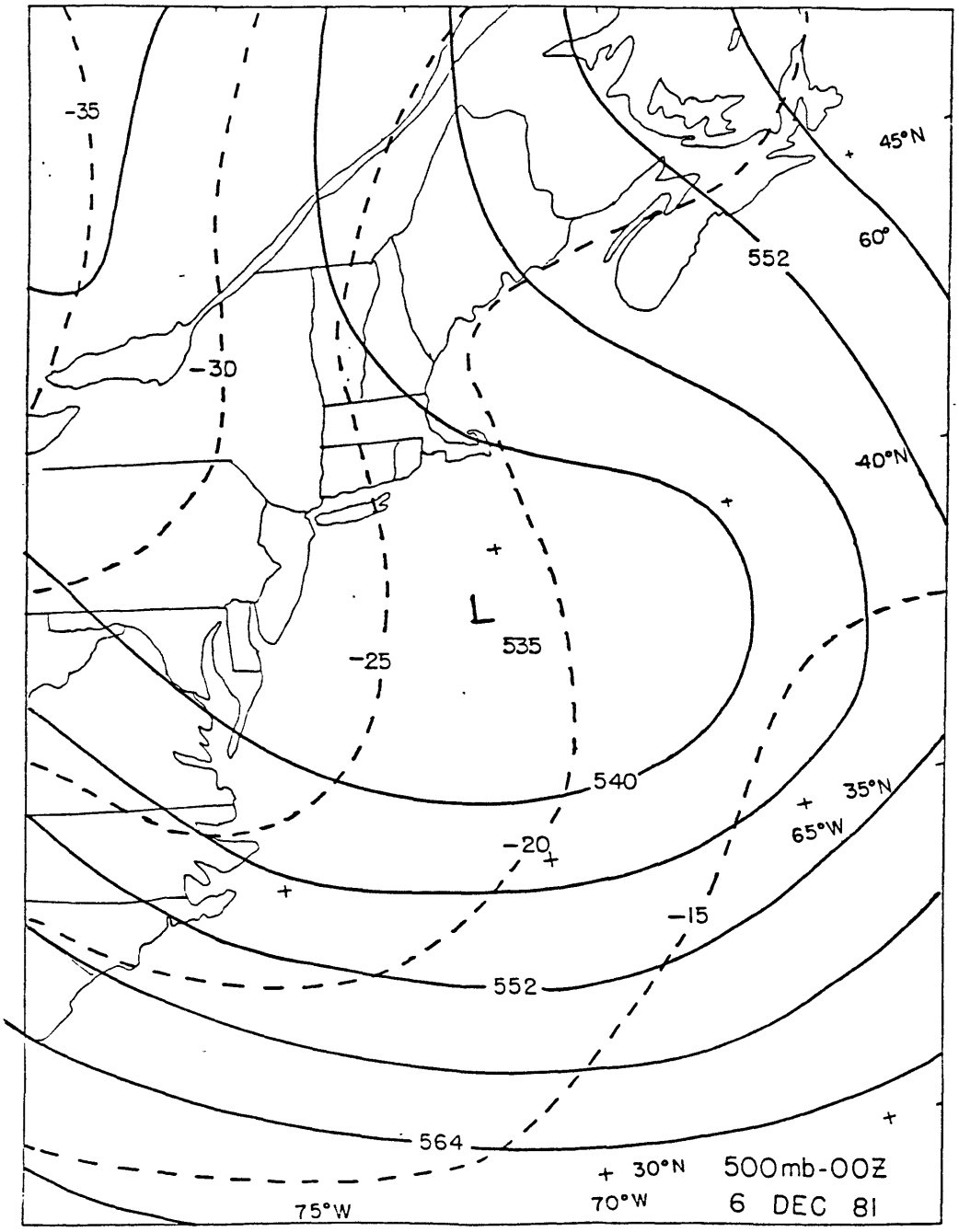

Fig. 5. 500 mb geopotential height (dam) and temperature (C) anlayses for 00GMT on 6 December 1981, adapted from NMC analyses.

particular band persisted for almost 14 hours in the New England area and produced snowfall rates of more than 2 inches per hour. A comparison of Figure 5 with Figure 3 shows that the band is embedded within the region of very strong shear. Analyses of potential temperature, equivalent potential temperature, and winds from a sounding at a location 60 km from the band are shown in Fig. 6. Again the region of strong shear is noted as is a deep layer of positive static stability that includes the layer of banded precipitation. There is no obvious frontal zone and there are no large regions of neutral stability. Most of the atmosphere is gravitationally stable. These observations would seem to rule out the occurrence of frontal precipitation, elevated convection or simple convective adjustment through upright convection.

While many of the band cases are not as striking as the one just described, most of them exhibit similar synoptic scale features. The presence of strong shear in all of the band cases makes symmetric instability a prime candidate for the mechanism responsible for the banded precipitation.

2.2 Mesoscale features of the cases studied.

In this section, the atmospheric conditions that existed in each case are presented. The cases are compared and the common features are deduced.

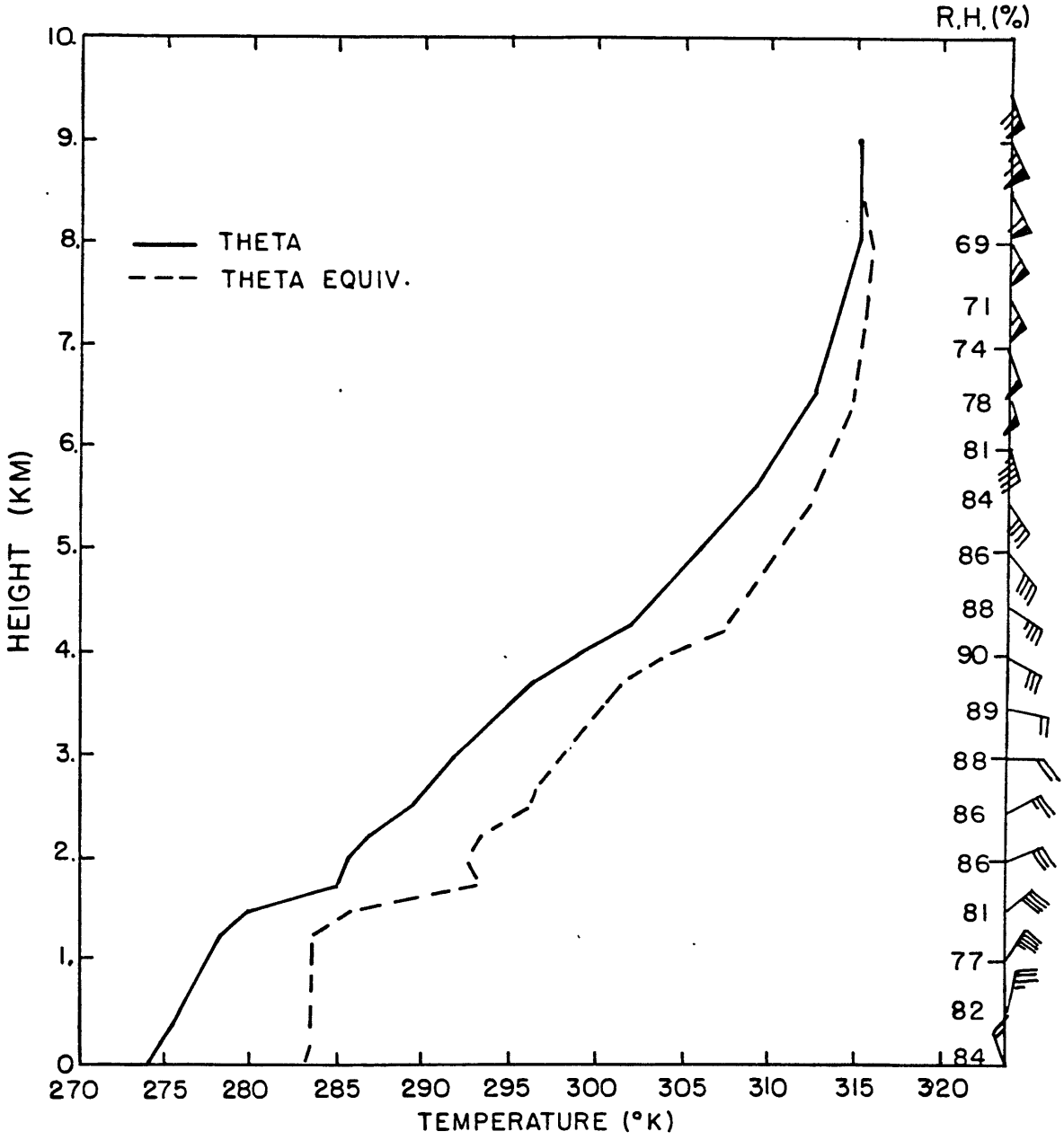

Fig. 6. Analyses of potential temperature (K), equivalent potential temperature (K), and winds from Portland, Me, at 00GMT on 6 December 1981.

As implied in the previous section, banded precipitation is often embedded in regions of strong shear. Table 1 lists for each case the shear direction, the shear magnitude, and the Brunt-Vaisalla frequency for dry and moist adiabatic ascent. All of these quantities are computed at the level of maximum wind-shear. Also shown are the magnitude of the 850-500 mb wind shear, the estimated bandedness, and the band orientation. The data used to make these calculations come from the sounding that was taken closest to the band.

On comparing the cases, a strong correlation between the bandedness and the maximum wind shear becomes apparent. The six cases classified with a level 2 or level 3 bandedness have a maximum wind-shear magnitude between 13 and 20 m/s per km. The remaining cases, classified as non-banded or weakly banded, with the exception of 4 December 1983 have a maximum wind shear magnitude between 7 and 12 m/s per km. A much weaker correlation is evident when the level of bandedness is compared with the magnitude of the 850-500 mb wind shear.

Fig. 7 is a scatter diagram of the band orientation versus the 1000-500 mb geostrophic shear direction and the shear direction at the level of maximum wind shear. All band cases judged non-zero are presented. The latter direction is averaged over a 1 km layer. The errors in measuring the geostrophic shear direction, and the mean

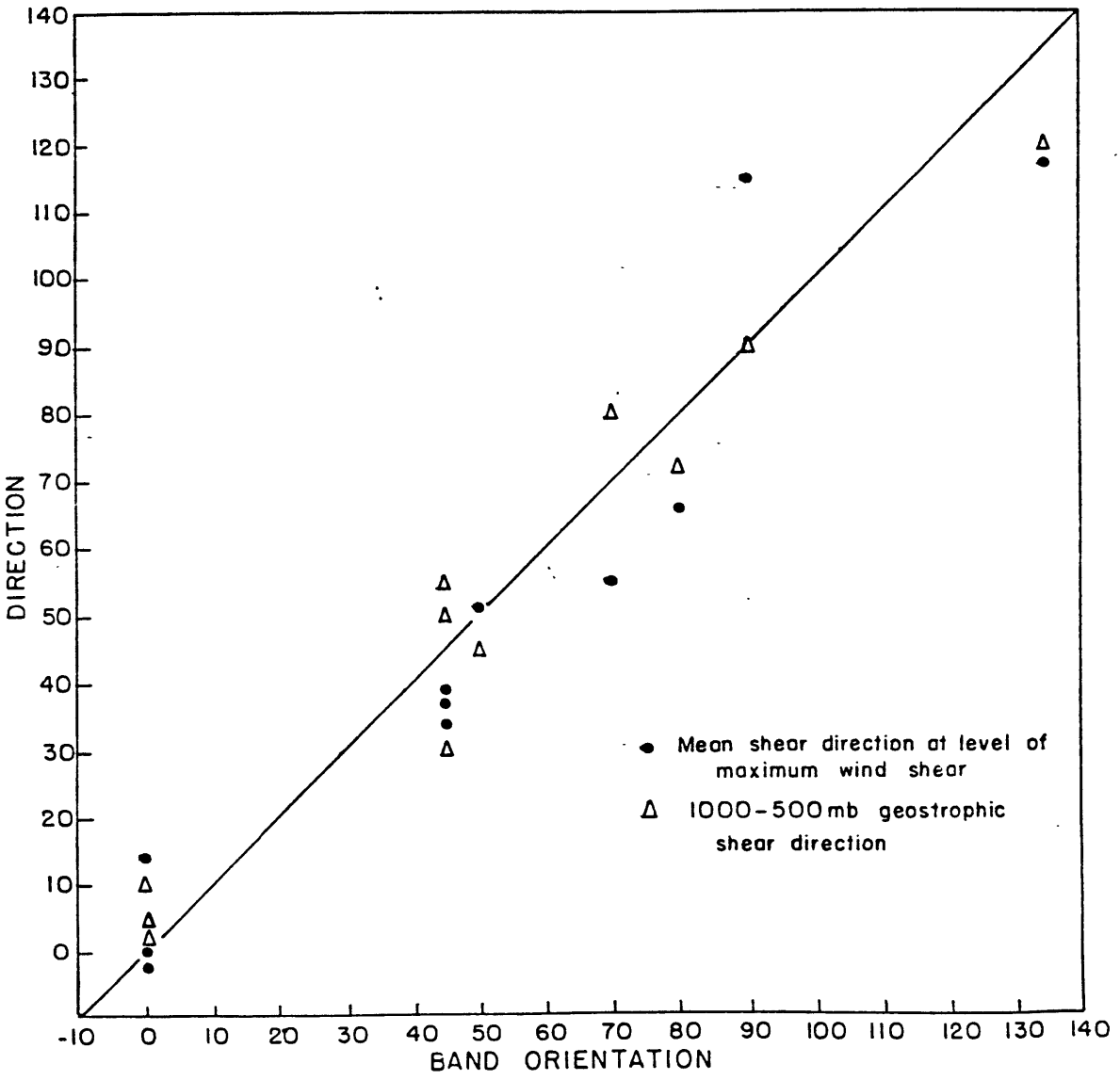

Fig. 7. Scatter diagram of the band orientation (deg) versus the 1000-500 mb geostrophic shear direction (deg) and the shear direction at the level of maximum wind shear.

shear direction are ±10 degrees and ±5 degrees respectively. The error in measuring the band orientation is ±10 degrees.

While both measures of the shear direction are close to the band orientation, the geostrophic shear direction is in better agreement. The RMS scatter is 9.2 degrees for the geostrophic shear direction versus 13.4 degrees for the shear direction at the level of maximum shear. In Table 1A, the total wind shear at the level of maximum shear and its component in the band-parallel direction are compared. Most of the wind shear is in the direction parallel to the band. In nine of the eleven band cases, the magnitude of the maximum wind shear, within the error in measurement, is equal to the band-parallel component. This underlines the result of Fig. 7 that the bands are aligned parallel to the wind shear direction.

Vertical profiles of the static stability were also analysed for each case. It was found that all of the cases were stable for dry adiabatic ascent above the boundary layer. In the region of maximum wind shear, three of the band cases show an atmosphere that is neutral or potentially unstable for moist adiabatic ascent. There are, however, other regions of the atmosphere in many of the cases that show indications of potential instability ($\partial\theta_e/\partial z<0$). A negative moist static stability is a sufficient condition

Table 1A

Case	Banded-ness	B.O.	LMSW	FFS	BP FFS
12/05/81	3	45	4.75	13.5	13.3
12/06/81	3	0	2.75	13.3	13.2
12/16/81	3	45	1.75	18.6	18.5
12/11/82	1	70	4.00	11.2	10.7
12/12/82	2	50	3.75	17.1	17.1
12/20/82	2	0	2.00	14.5	14.5
01/11/83	3	0	3.00	19.4	17.8
01/24/83	0	-	4.25	8.2	-
02/03/83	0	-	3.25	7.9	-
02/12/83	3	80	5.50	13.4	13.0
11/28/83	3	135	2.75	21.2	18.5
12/03/83	1	90	5.75	11.5	11.3
12/04/83	0	-	5.25	22.4	-
12/06/83	0	-	2.00	9.6	-
01/11/84	2	45	3.75	19.5	19.3

LMSW - level of maximum wind shear magnitude [km]
B.O. - band orientation [deg]
FFS - wind shear magnitude [m/s/km]
BP FFS - band-parallel wind shear magnitude [m/s/km]

Note: FFS, BP FFS, computed at LMWS

for convective overturning only if the atmosphere is saturated. For the cases considered in this study, the regions of potential instability that were judged saturated are weakly unstable and can be considered, within the error of measurement, to be neutral. Regions that are assessed as having substantial potential instability are in all cases associated with humidity gradients. In this instance, the atmosphere is not uniformly saturated and the potential instability may never be released. When comparing the static stability with the bandedness, no correlation for either dry or moist conditions is apparent. This lack of correlation, however, does not preclude the possibility that potential instability may play a role in the formation of the precipitation bands considered in this paper.

Some evidence has already been given to justify the assumption that the bands are two-dimensional in nature. The bands are observed to be aligned close to the geostrophic shear vector which, in a geostrophically balanced atmosphere, is the direction perpendicular to the average temperature gradient. The band's thermodynamic properties can therefore be approximated as having most of their variations in the cross-band direction. In addition, Doppler radar and synoptic scale wind analyses provide evidence that most of the flow is in the band-parallel direction with variations in this flow occurring predominantly in the cross-band direction.

As remarked earlier, it is the fact that the bands appear to be associated with strongly sheared flow in a stable or near-neutral atmosphere which provides the motivation for considering symmetric instability as a primary mechanism. The two-dimensional nature of the bands also justifies the application of simple models of symmetric instability and as will be shown in the following section, the observations can be used to support many of the assumptions made in the theoretical models.

3. Comparisons between theory and observations.

The observations presented in the previous section support the use of simple linear theory and parcel theory in assessing the symmetric instability of the atmosphere. Most of the horizontal variations in thermodynamic and kinematic properties are observed to be in the cross-band direction. The bands can, to a good approximation, be considered to be two-dimensional. The observed bands were always associated with very strong vertical shear of the band-parallel wind component.

3.1 The assessment of symmetric instability

In Section 1, two techniques were discussed for assessing the symmetric stability of the atmosphere. One technique is to calculate the symmetric stability parameter $(\eta/f)\cdot Ri$ from observations. Where this parameter is less than unity, the atmosphere is symmetrically unstable to infinitesimal perturbations from the geostrophically-balanced basic state. If the atmosphere is saturated, the effect of latent heat can be included by replacing the potential temperature with the equivalent potential temperature in the expression for Ri.

The second technique is based on the parcel method derived by Emanuel (1983). The environment surrounding a given parcel is assumed to be in geostrophic balance. The parcel's stability can be assessed by imagining its disp-

lacement from an equilibrium state and by evaluating the net acceleration of the parcel resulting from the imbalance in pressure gradient, Coriolis and buoyancy forces between the parcel and its environment.

The stability of the atmosphere to parcel displacements can be assessed in two ways depending on the quality of the observational base. Given adequate sounding coverage across a band, a vertical cross-section of θ and M can be constructed. Then, as shown in section 2, parcels are unstable to symmetric overturning where M surfaces are more shallow than θ surfaces.

The parcel stability can also be approximately assessed from a single sounding. This method is similar to the analysis of upright convection on a tephigram. Given an atmospheric sounding of temperature and winds, the parcel stability is assessed by adiabatically lifting a parcel and modifying the lifted parcel temperature by adding the value

$$\frac{1}{2}\frac{T_{v_p}}{g}\frac{f}{\eta}\frac{\partial}{\partial z}\left\{(V-V_p)^2\right\}$$

where v is the environmental velocity and v is the initial velocity of the parcel.

Stability analyses based on a single sounding were done for all cases. Multiple soundings across a band from which vertical cross-sections could be constructed were available in only three of the band cases. Stability

analyses from a single-sounding require the knowledge of the absolute vorticity, $\eta=f+\partial v/\partial x$ as a function of height. For the cases considered in this study, the relative vorticity $\partial v/\partial x$ appears to have a small effect on the stability. The relative vorticity was estimated from LFM 500mb vorticity fields for all cases. It was found that neglecting $\partial v/\partial x$ in the Richardson number analysis would lead to an error of only about ten percent. For this reason, the relative vorticity is neglected in the single-sounding stability analyses.

3.2 An example of the assessment techniques as applied to a single sounding.

The sounding used in this example was taken from Chatham, Massachusetts at 12 GMT, on 5 December, 1981. At this time, a snow band (judged level 3) was observed in the vicinity of Chatham. As the band moved over Chatham approximately three hours later, the band orientation was 045 degrees.

Fig. 8a-d shows vertical profiles of Ri^{-1}, θ, θ_e, and the magnitude of the component of wind shear parallel to the band. Ri is calculated from the observed band-parallel wind shear, which is considered to represent the geostrophic basic state, and dry adiabatic ascent is assumed. Note that the layer between 4.0 and 6.0 km is nominally symmetrically unstable. The potential temperature and equivalent poten-

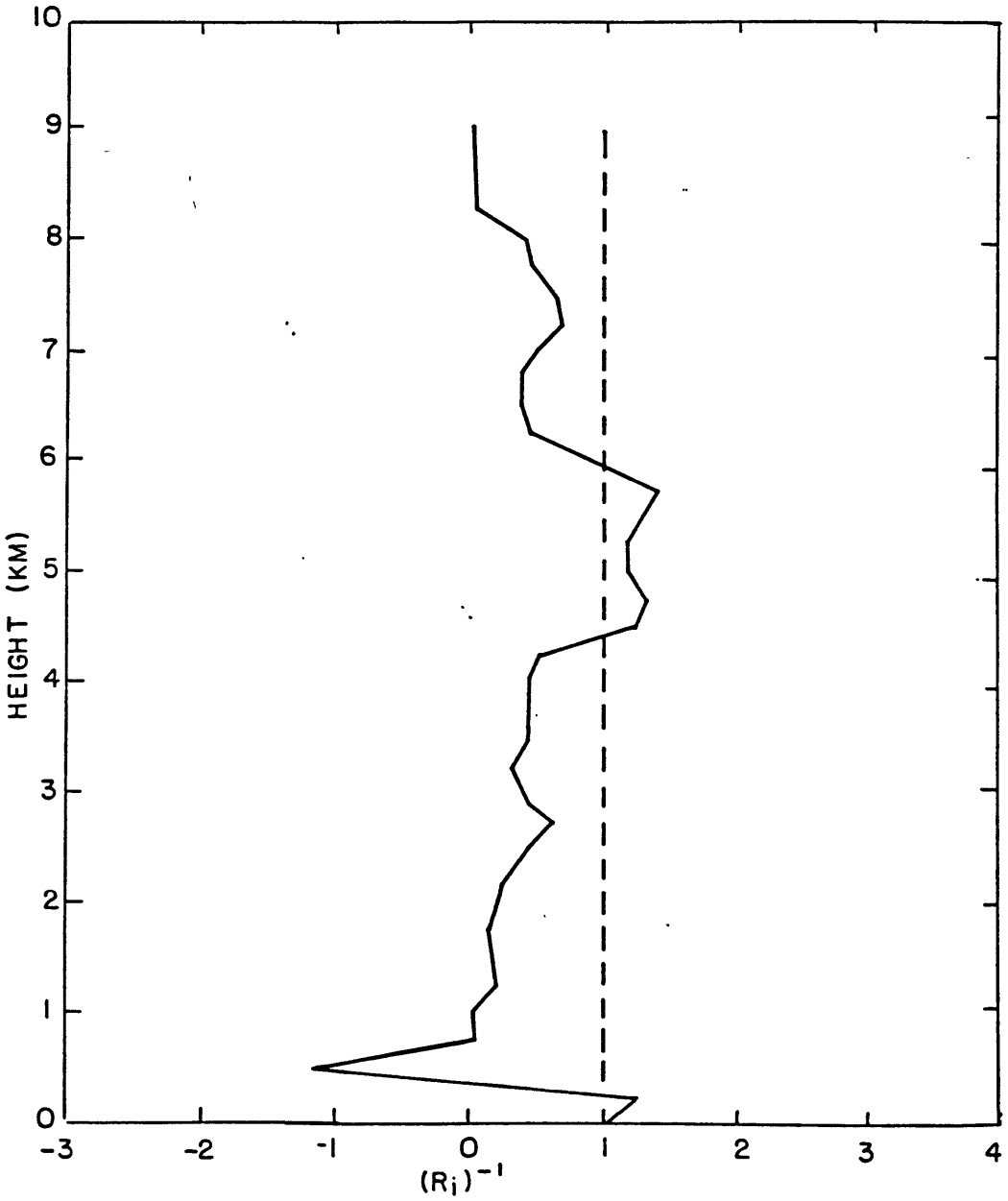

Fig. 8 a-d. Plots of (a) inverse Richardson number, (b) potential temperature (K), (c) equivalent potential temperature (K), and (d) the magnitude of the band-parallel wind shear (m/s/km) as a function of height (km).

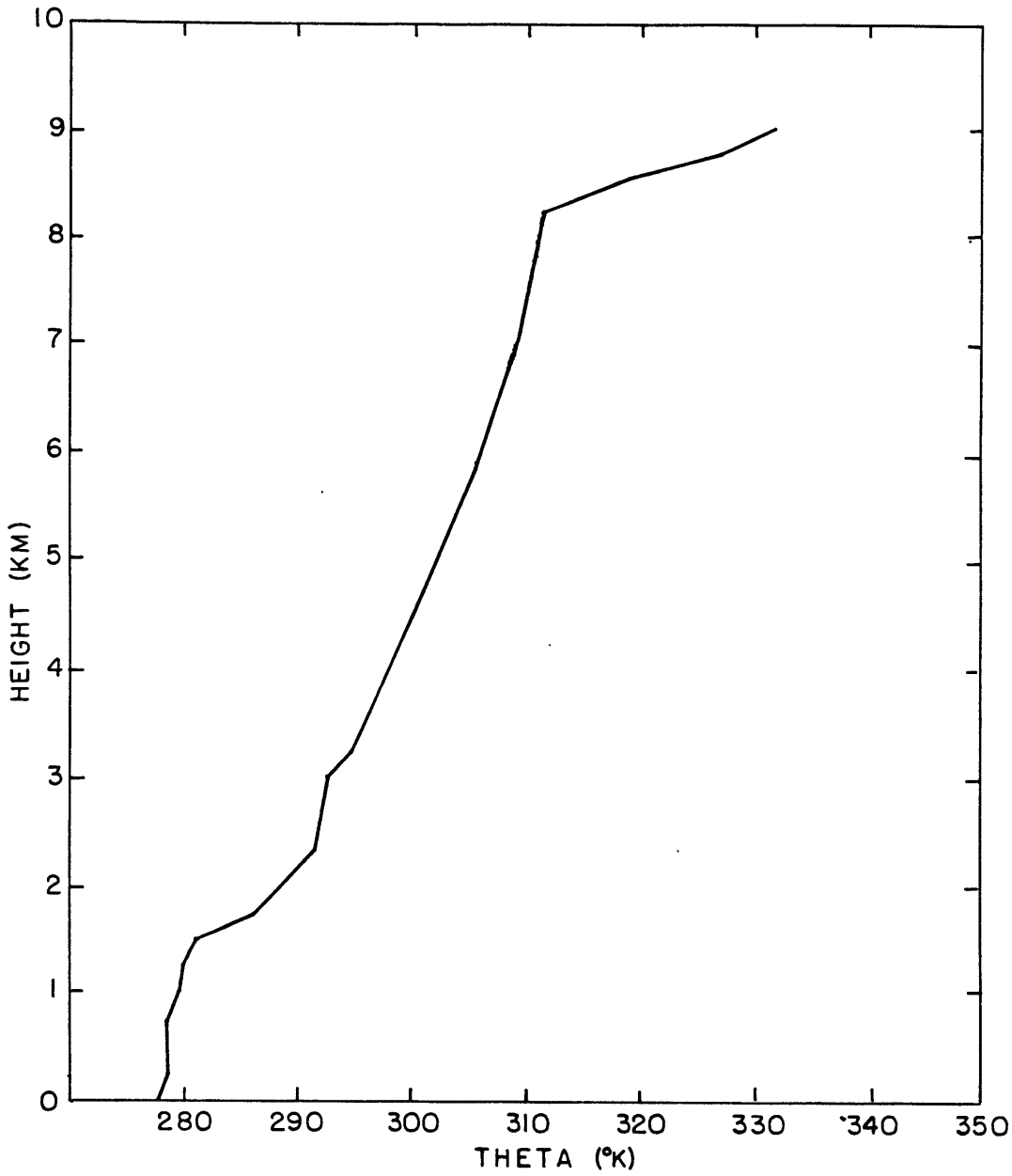
10
9
8
7
6
5
4
3
2
1
0
HEIGHT (KM)
280
290
300
310
320
330
340
350
THETA (°K)

Fig. 8b

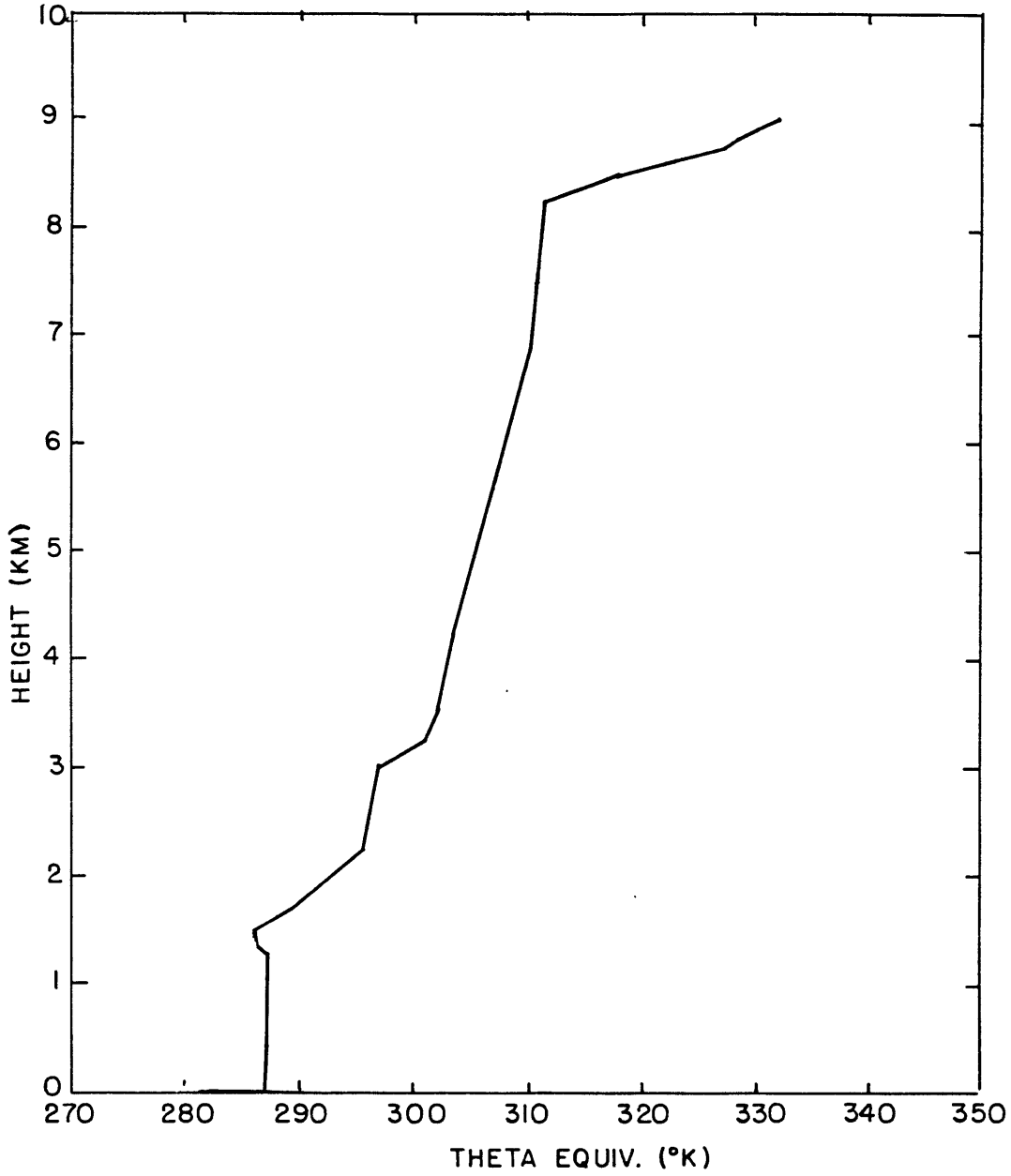
10
9
8
7
6
5
4
3
2
1
0
HEIGHT (KM)
270
280
290
300
310
320
330
340
350
THETA EQUIV. (°K)

Fig. 8c

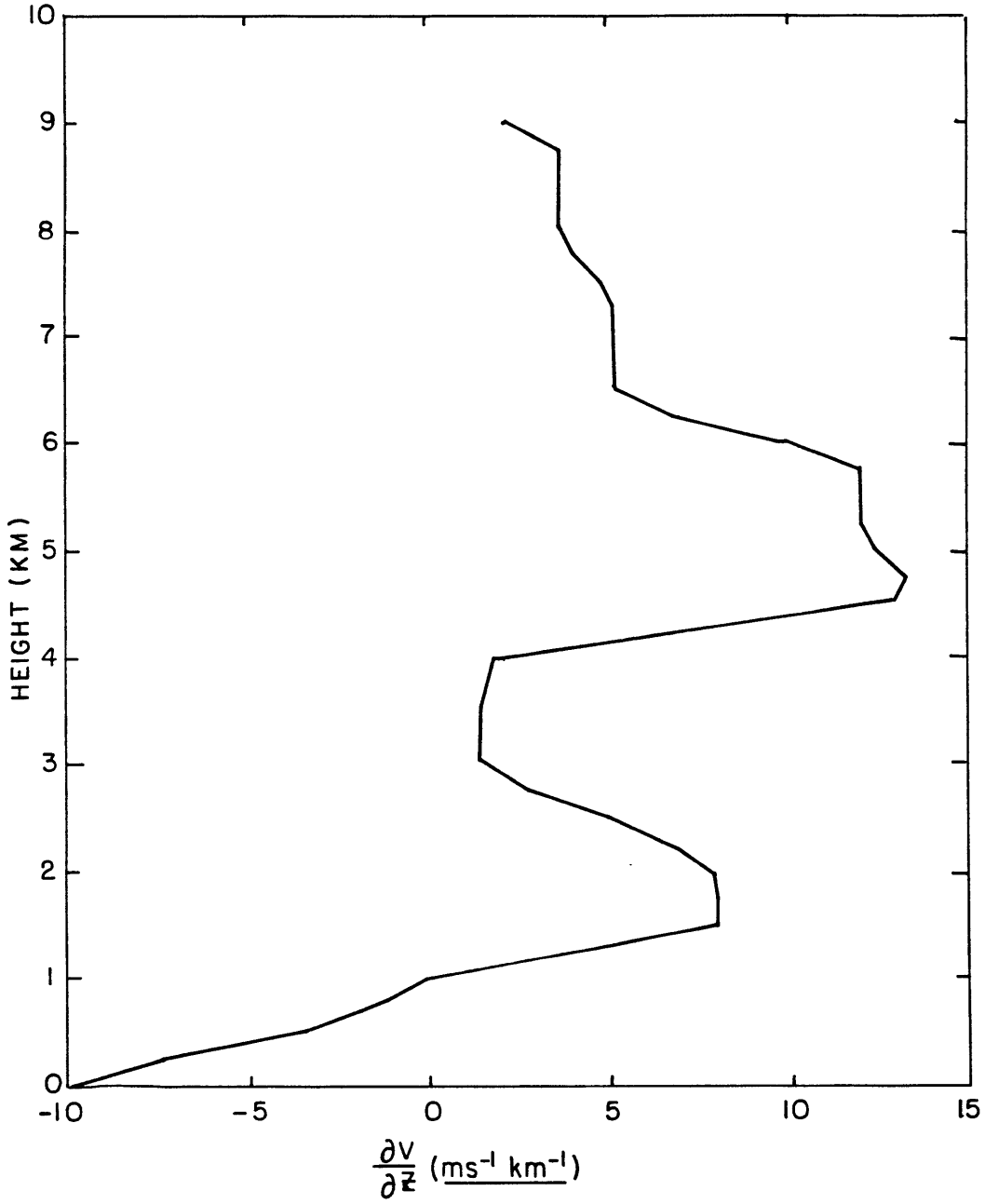
HEIGHT (KM)
10
9
8
7
6
5
4
3
2
1
0
-10
-5
0
5
10
15
$\frac{\partial V}{\partial z}$ (ms^{-1} km^{-1})

Fig. 8d

tial temperature profiles, on the other hand, show that the atmosphere is stable for both dry and moist adiabatic ascent. The profile of the shear magnitude indicates that the subcritical Richardson numbers between 4.0 and 6.0 km result from the very strong shear in this layer.

The parcel method for this case is illustrated in Fig. 9. Plotted is the modified parcel temperature for the slantwise adiabatic ascent of an air parcel originating at 4.0 km height. The orientation of the parcel is assumed to be along the band-parallel direction (045°/225°). (Recall that a parcel refers to an infinitely long tube oriented along the direction of the band.) Also shown are the environmental and dewpoint temperatures, and the 283°K moist adiabat that passes through the parcel's starting position. Conventional gravitational instability is evaluated by lifting the parcel vertically along its appropriate moist or dry adiabat and comparing the parcel temperature to the environment. Symmetric instability is evaluated by lifting the parcel along the line of slantwise ascent (labeled parcel temperature in the figure) and making the same temperature comparison. This analysis shows that while parcels originating near 4.0 km are completely stable to vertical displacements, they are unstable to slantwise displacements up to a height of 6.25 km.

Fig. 10 shows contours of the maximum temperature difference between a parcel and its environment during

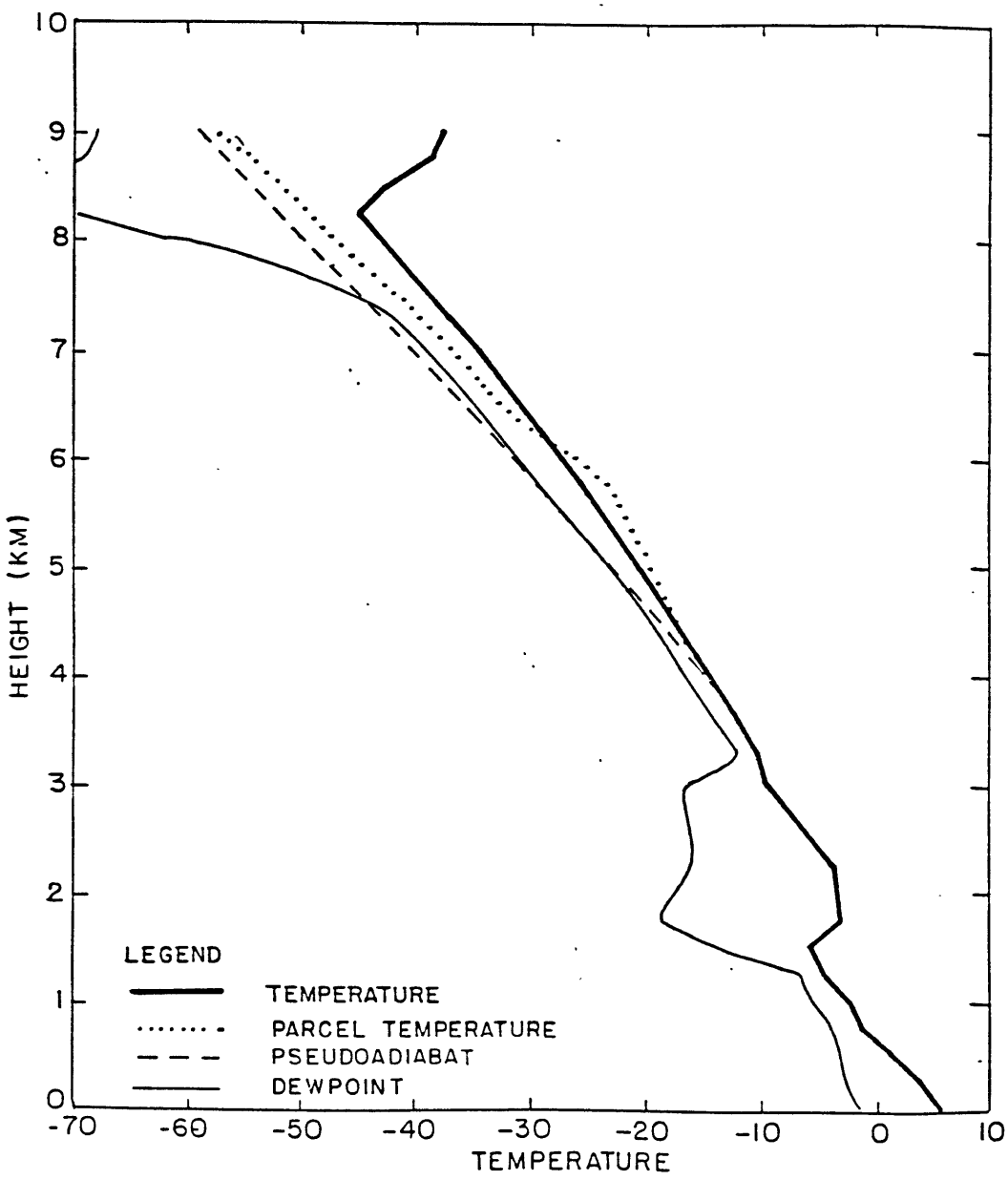

Fig. 9. Plots of the modified parcel temperature (C) for the slantwise ascent of an air parcel originating at 4.0 km height, the environment and dewpoint temperature (C), and the 283K moist adiabat that passes through the parcel's starting position. The orientation of the parcel is assumed to be along the band-parallel direction (045°/225°).

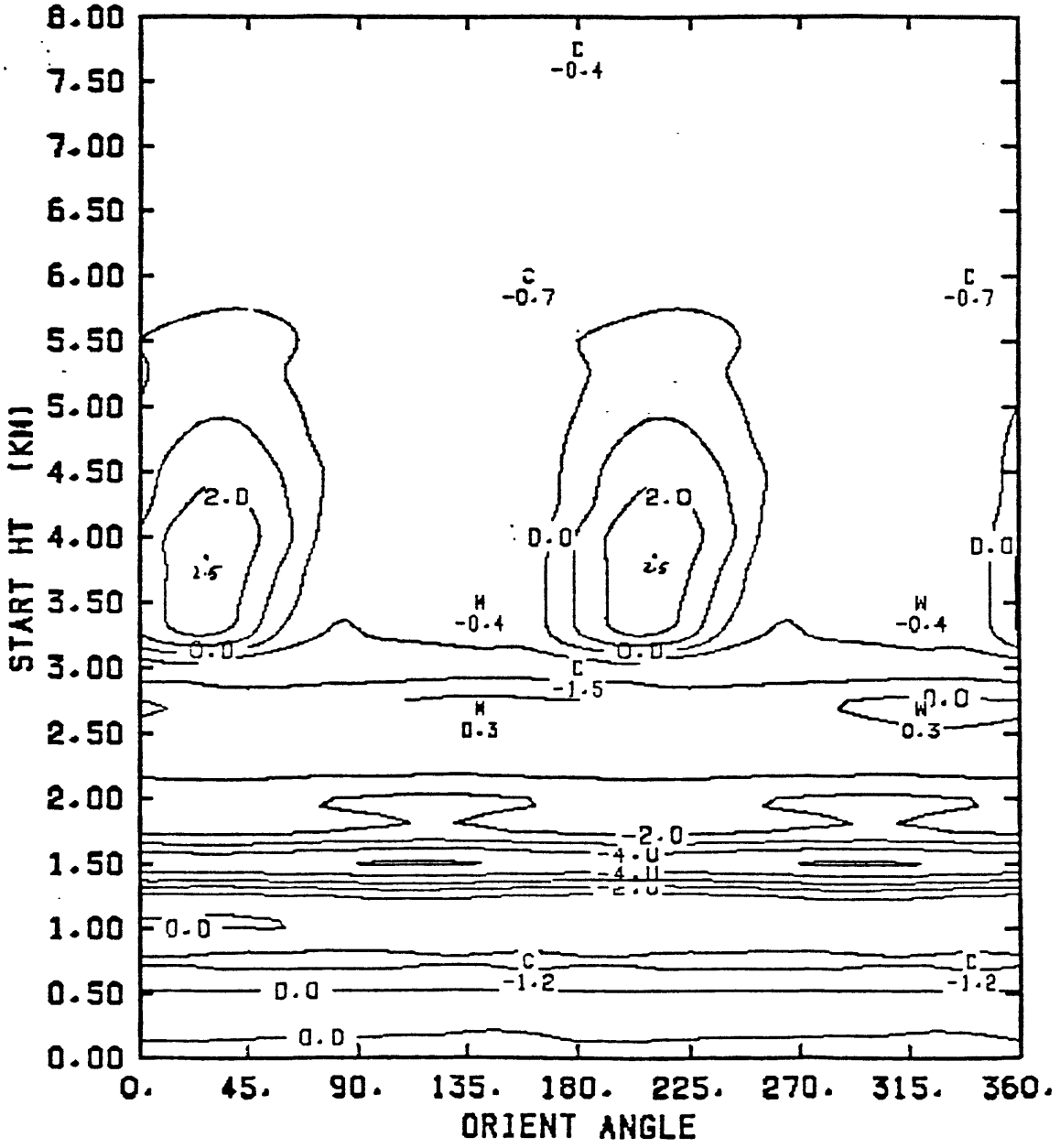

Fig. 10. Contours of the maximum temperature difference (C) between a parcel and its environment during lifting to 9.5 km as a function of starting height (km) and parcel orientation (deg).

lifting to 9.5 km for different starting heights and parcel orientations. There is a well-defined maximum of 2.5°C at a height of 4.0 km for an orientation angle of 030°/210°. The analysis further indicates that all parcels originating between 3.25 and 5.5 km with an orientation angle between 30 and 60 degrees are unstable to slantwise lifting. The depth and height of the layer of maximum symmetric instability agree with the Richardson number analysis.

3.3 Results of single-sounding analyses.

The parcel method can be used to predict the strength and orientation of banded precipitation. In the above example, parcel theory predicts that the band will be oriented at 030°/210°. The strength of the band should be related to the predicted parcel temperature surplus. The actual correlation between this temperature surplus and bandedness will be examined after assessing the symmetric stability for all band cases.

Table 2 lists for each band case the minimum value of the Richardson number for dry and moist adiabatic ascent and descent, and the level of the minimum dry Richardson number. Notice that in three of the cases, the Richardson number for moist ascent is equal to or greater than it's corresponding value for dry ascent. This is due to the presence of humidity gradients that result in a static stability for moist ascent that is greater than that for dry

Table 2.

Case	Banded-ness	B.O.	LMWS	LMI	Ri dry	Ri moist
12/05/81	3	45	4.75	5.00	.76	.46
12/06/81	3	0	2.50	2.50	.93	.93
12/16/81	3	45	1.75	1.75	.58	.32
12/11/82	1	70	4.00	none	1.93[1]	1.53[1]
12/12/82	3	50	3.75	4.00	0.43	-0.11
12/20/82	2	0	2.00	2.00	0.32	-1.79
01/11/83	3	0	3.00	3.00	0.79	0.78
01/24/83	0	-	4.25	none	5.10[1]	1.90[1]
02/03/83	0	-	5.50	none	5.49[1]	8.45[1]
02/12/83	3	80	5.50	5.25	0.68	0.34
11/28/83	3	135	2.75	2.75	0.86	1.23
12/03/83	1	90	5.75	5.75	0.62	0.29
12/04/83	0	-	5.25	5.25	0.55	0.44
12/06/83	0	-	2.00	none	1.13[1]	1.24[1]
01/11/84	2	45	3.75	3.75	0.92	0.94

[1] - value calculated at LMWS

B.O. : band orientation [deg]
LMWS : level of maximum wind shear [km]
LMI : level of maximum instability [km]

ascent. Except for regions of potential instability to upright convection, the level of minimum Richardson number is the same for both dry and saturated conditions. For comparison to Table 1, many of the parameters listed there are included in Table 2. The parameters listed are computed at the level of minimum Richardson number calculated for dry ascent. This level will subsequently be referred to as the level of maximum instability (LMI). The boundary layer up to 1.5 km is excluded from all calculations in an attempt to exclude regions where surface viscous forces are important. In these regions the inviscid theory may not be valid.

It is immediately evident that in all but one case, the LMI is within 250 meters of the level of maximum wind shear. This implies that the indications of symmetric instability result from the strong shear. Any change in static stability with altitude has only a small effect on the level of the critical Richardson number. The positive correlation between bandedness and maximum shear magnitude that was observed in Section 2 is therefore essentially the same as the positive correlation between bandedness and minimum Richardson number that is evident in Table 2.

Table 3 summarizes the assessment of symmetric instability by the single sounding parcel method for all cases studied. The same analysis technique used with Fig. 10 is applied. Parcels are lifted slantwise from starting levels between 1.5 and 7 km to a height of 9.5 km for all

Table 3.

Case	Banded-ness	B.O.	LMI	MTS	LMTS	P.O.	LUP
12/05/81	3	45	4.75	2.5	3.75	30	3.25-5.50
12/06/81	3	0	2.50	2.8	2.25	0	2.00-2.50
12/16/81	3	45	1.75	1.2	1.50	40	1.50-1.75
12/11/82	1	70	4.00	0.0	3.00	*	**
12/12/82	2	50	3.75	6.0	3.50	60	3.00-5.00
12/20/82	2	0	2.00	2.1	1.50	-10	1.50-2.00
01/11/83	3	0	3.00	3.2	1.75	20	1.50-2.50
01/24/83	0	-	4.25	0.2	7.00	140	7.00
02/03/83	0	-	3.25	1.1	5.50	130	5.50
02/12/83	3	80	5.25	4.7	3.50	45	2.50-5.25
11/28/83	3	135	2.75	6.4	2.25	120	1.75-3.75
12/03/83	1	90	5.75	0.8	5.00	110	4.50-6.00
12/04/83	0	-	5.25	1.7	4.75	*	4.50-6.50
12/06/83	0	-	2.00	-0.5	3.50	*	**
01/11/84	2	45	3.75	2.7	2.75	50	1.50-3.50

B.O. : band orientation [deg]
LMI : level of maximum instability [km]
MTS : maximum parcel temperature surplus [deg C]
LMTS : level of MTS [km]
P.O : predicted orientation angle [deg]
LUP : layer of unstable parcels [km]

* - no preferred orientation
** - no unstable parcels

possible band orientations. From the resulting plots the following quantities are read and listed in Table 3: level and magnitude of maximum parcel-temperature surplus, prediction of band orientation, and layer of unstable parcels. In eight of the eleven band cases, the LMI determined from Richardson number analyses is within the layer of unstable parcels. In two band cases the LMI is within 500 meters of this layer. One band case has no LMI. There appears to be a preference for the stronger band cases to have a larger maximum parcel temperature surplus and a deeper layer of instability.

Fig. 11 shows the actual band orientation, the predicted orientation and the 1000-500 mb geostrophic shear direction. The predicted orientation angle is calculated to the nearest 10 degrees. In only six of the eleven band cases, the predicted orientation angle is as close or closer to the band orientation than the 1000-500 mb geostrophic shear direction. Using the parcel method stablity analysis to predict the band orientation is slightly worse than simply using the 1000-500 mb geostrophic shear direction.

Other comparisons can be made with the linear theory. Recall that linear theory predicts that the spacing between bands should be related to the depth of the unstable region and to the slope of the isentropes. An order of magnitude for this predicted wavelength can be obtained from a simple scaling analysis. Let H be the depth of the unstable

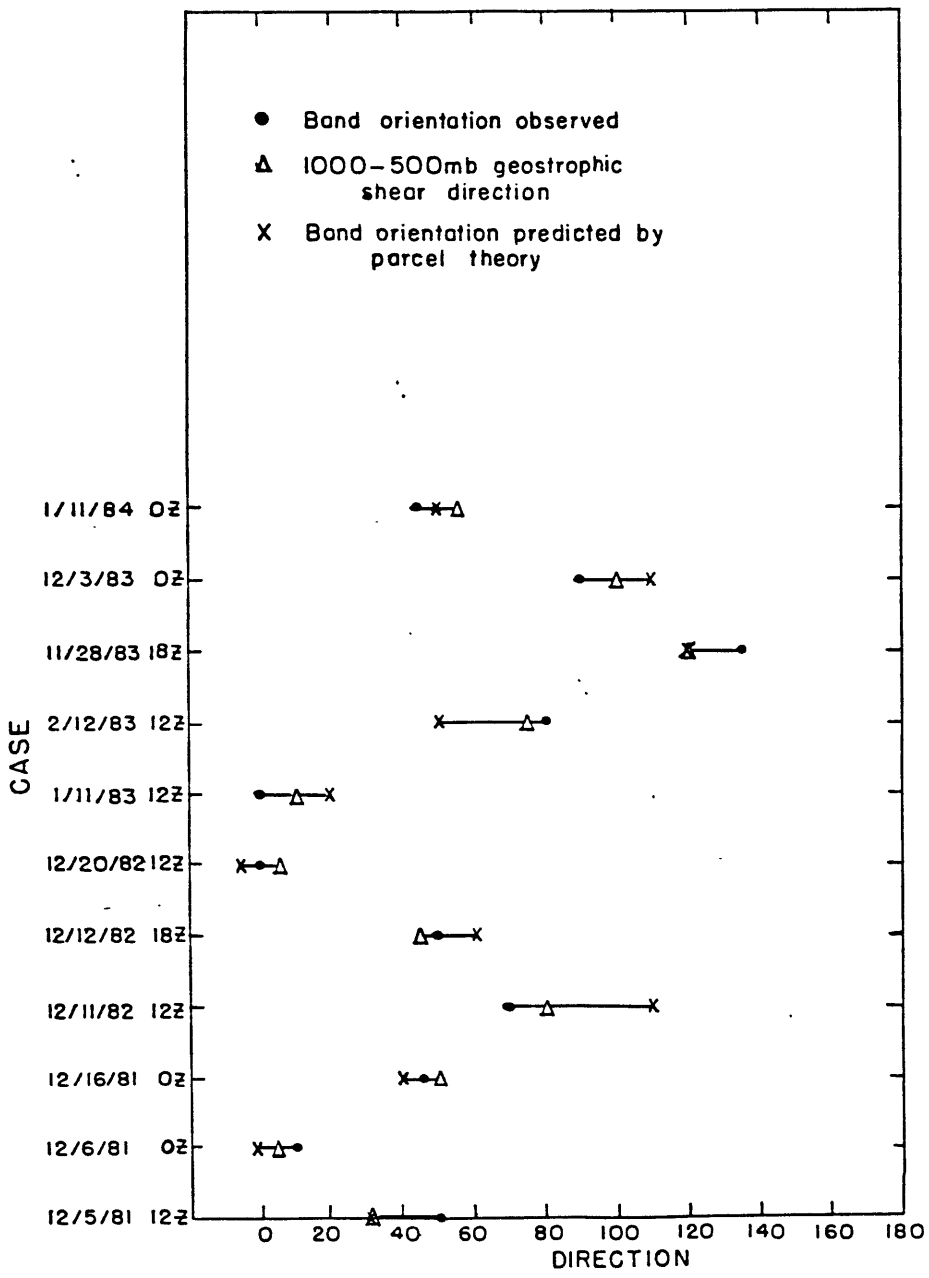

Fig. 11. Comparison of the actual band orientation, the predicted orientation, and the 1000-500 mb geostrophic shear direction for each band case.

region. The slope α of the isentropes is given by

$$\alpha = \frac{-\frac{\partial \theta}{\partial z}}{\frac{\partial \theta}{\partial x}} . \qquad (3.1)$$

Thus the predicted wavelength L can be approximated by

$$L \sim \frac{H}{|\alpha|} . \qquad (3.2)$$

If the thermal wind relation is used to express the horizontal temperature gradient in terms of the geostrophic wind shear, L can be written in finite difference form as

$$L \sim \frac{Hg}{f\bar{\theta}} \frac{\Delta\theta}{\Delta V}\bigg|_H , \qquad (3.3)$$

where $\Delta\Theta$ and ΔV are evaluated across the level of maximum instability.

Multiple bands were observed in four of the band cases. The observed wavelength was measured from radar reflectivity factor maps. Table 4 shows that the wavelength predicted by Eq. 3.3 agrees well with the observed wavelength in three of the four cases.

The present linear theory also implies that the bands should not propagate relative to the mean flow in the unstable region. Figs. 12 a-e show the observed speed of the band along with vertical profiles of the observed cross-band wind speed for the five bands judged level 3 (bandedness). The level 3 band cases were chosen for this comparison because they were the easiest to follow in time.

Table 4.

Case	Observed Wavelength (km)	Predicted Wavelength (km)
12/12/82	45	56
01/11/83	55	71
11/28/83	115	120
01/11/84	65	164

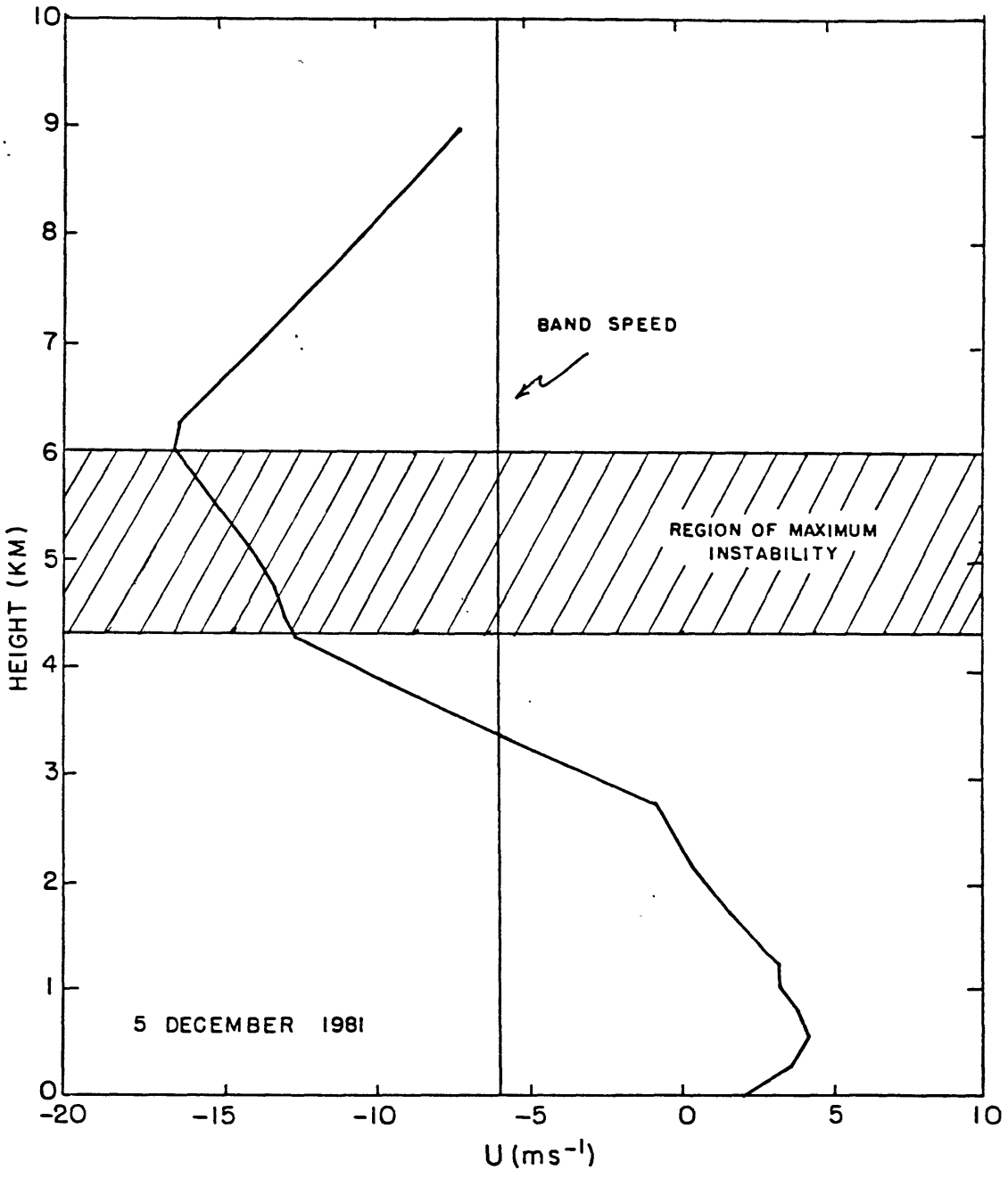

Fig. 12 a-e. The observed cross-band wind speed (m/s) as a function of height (km) for (a) 12GMT, 5 December 1981, (b) 00GMT, 16 December 1981, (c) 12GMT, 11 January 1983, (d) 12GMT, 12 February 1983, (e) 18GMT, 28 November 1983.

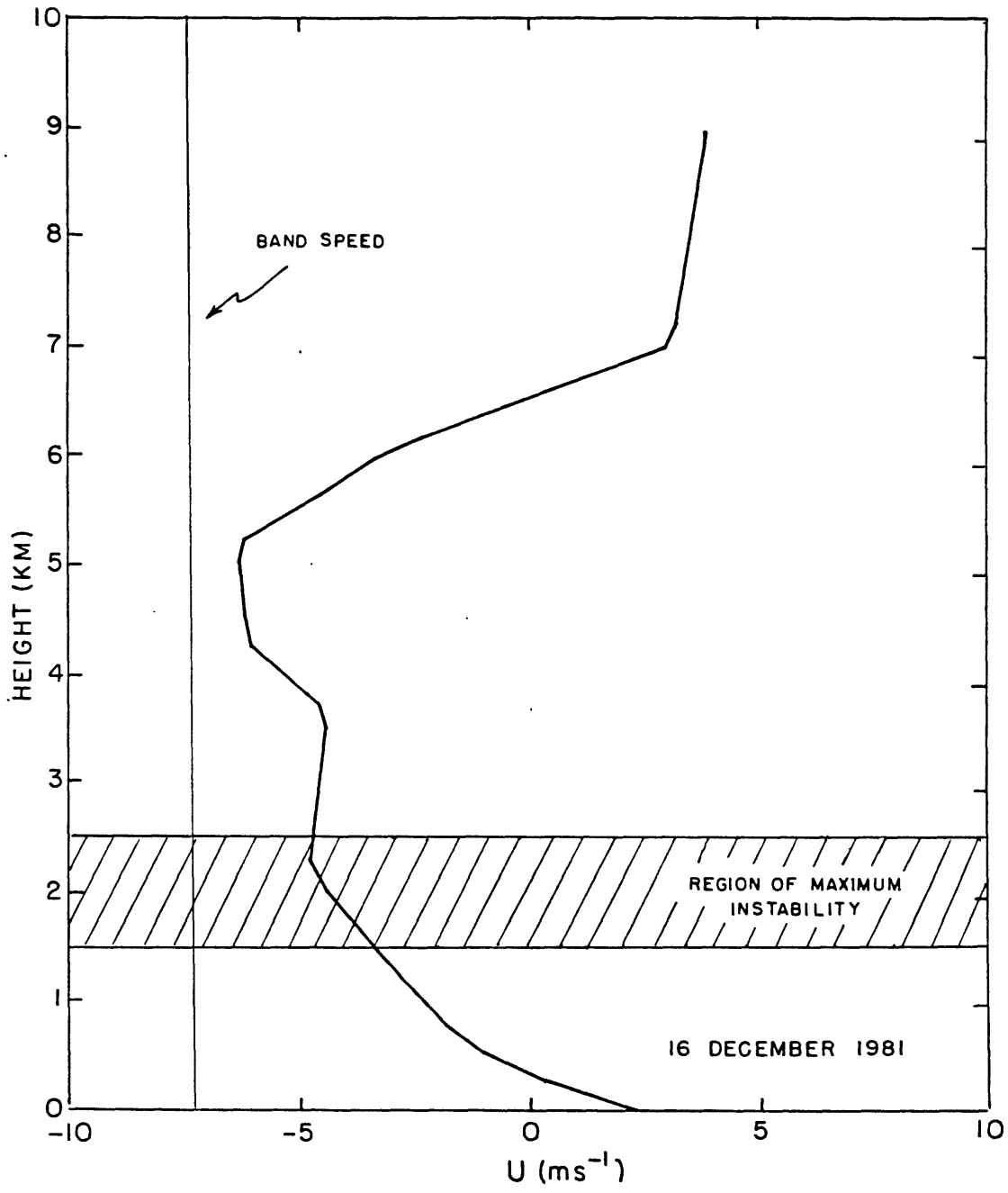
10
9
8
7
6
5
4
3
2
1
0
HEIGHT (KM)
BAND SPEED
REGION OF MAXIMUM
INSTABILITY
16 DECEMBER 1981
-10
-5
0
5
10
U (ms^{-1})

Fig. 12b

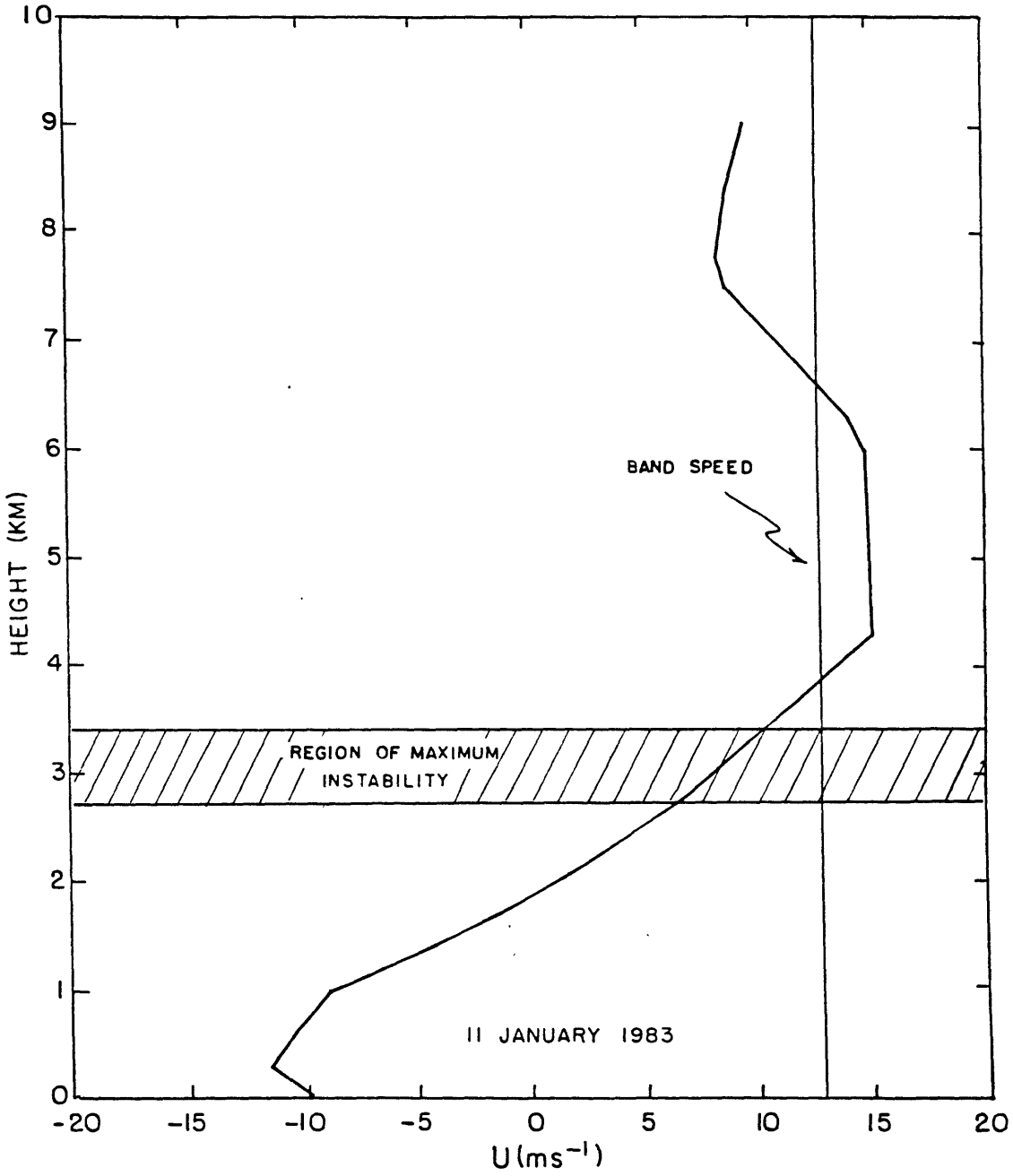
10
9
8
7
6
5
4
3
2
1
0
HEIGHT (KM)
BAND SPEED
REGION OF MAXIMUM
INSTABILITY
11 JANUARY 1983
-20
-15
-10
-5
0
5
10
15
20
U(ms⁻¹)

Fig. 12c

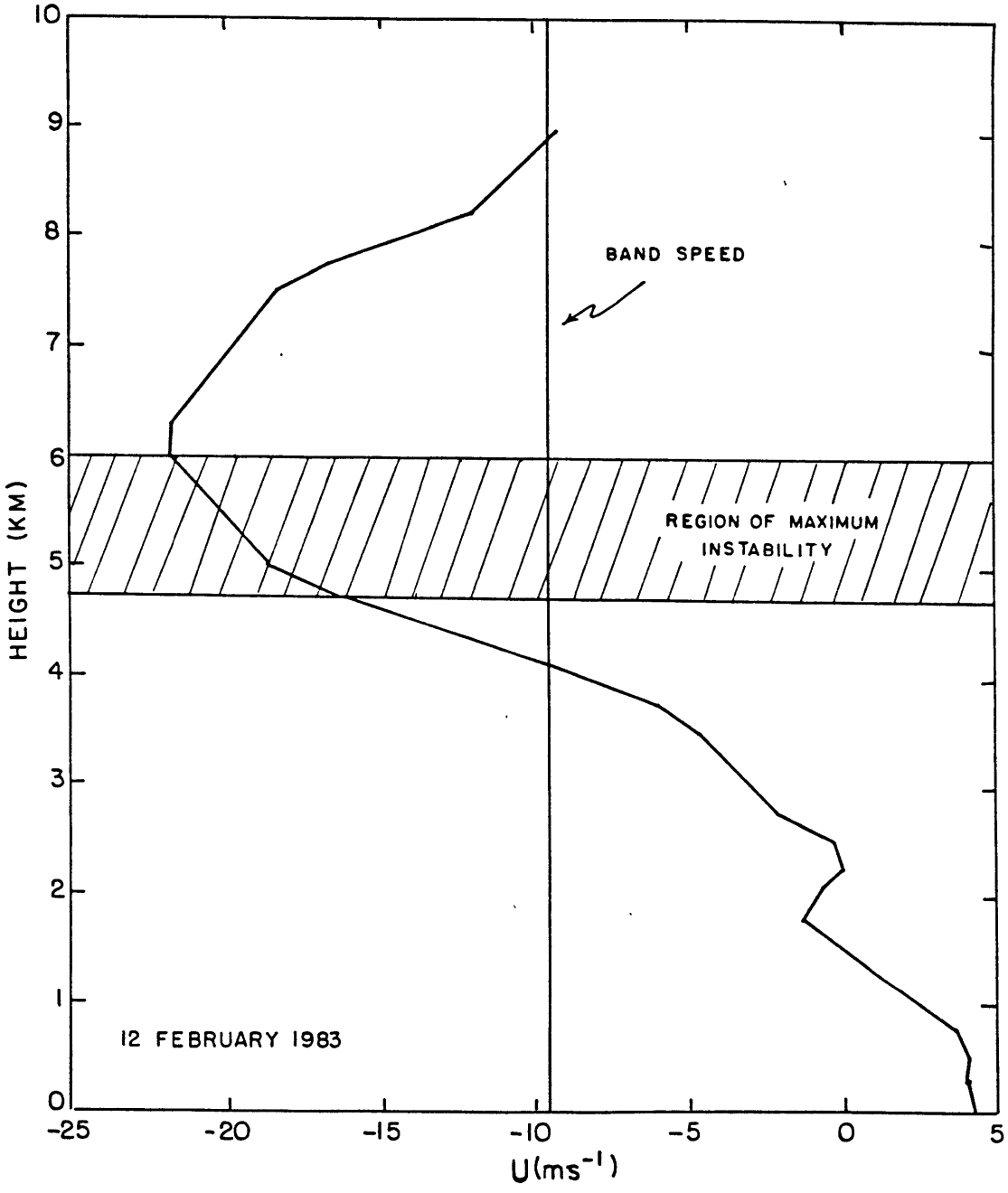
10
9
8
7
6
5
4
3
2
1
0
HEIGHT (KM)
BAND SPEED
REGION OF MAXIMUM
INSTABILITY
12 FEBRUARY 1983
-25
-20
-15
-10
-5
0
5
U(ms⁻¹)

Fig. 12d

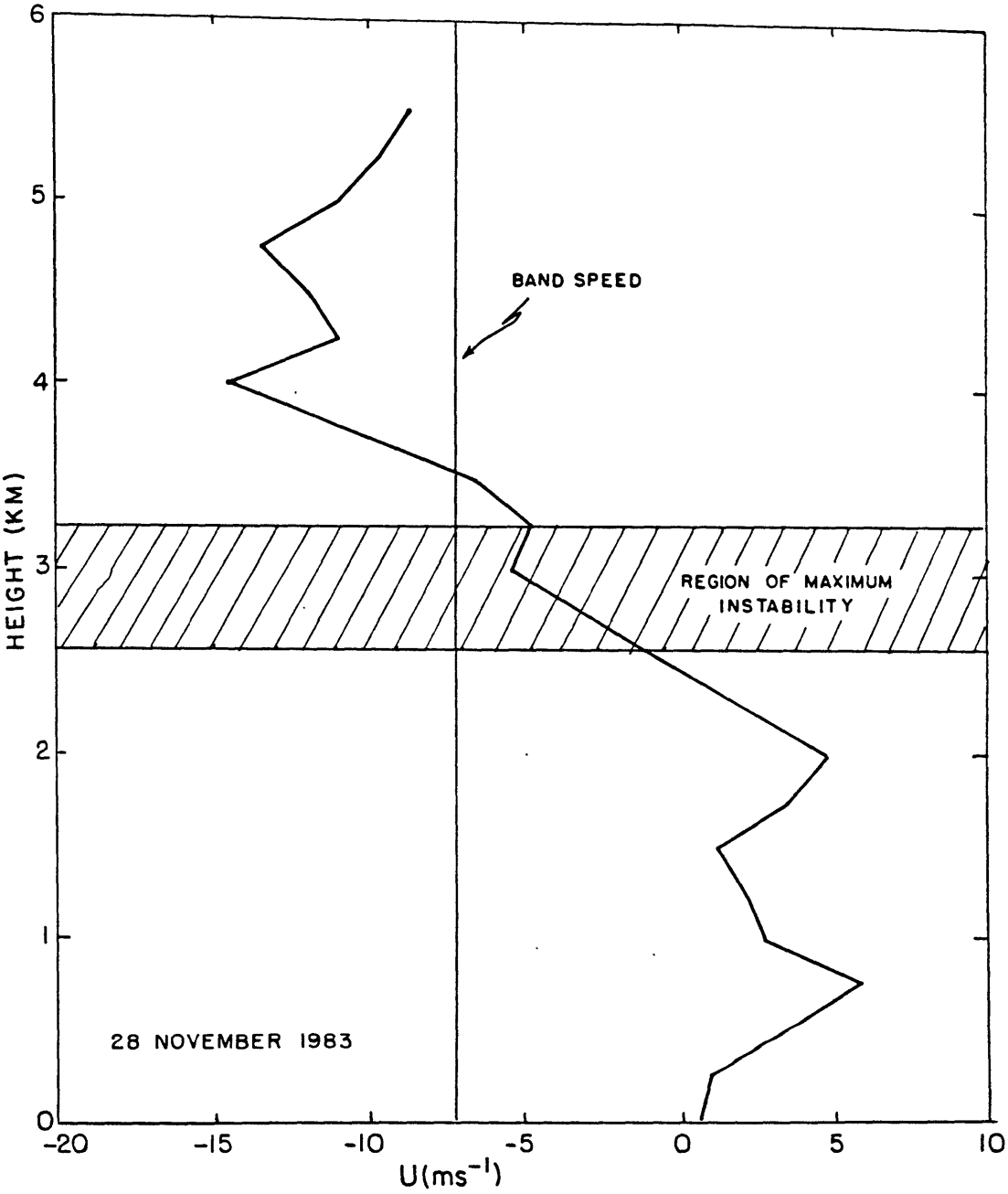
6
5
4
3
2
1
0
HEIGHT (KM)
BAND SPEED
REGION OF MAXIMUM
INSTABILITY
28 NOVEMBER 1983
-20
-15
-10
-5
0
5
10
U(ms^{-1})

Fig. 12e

The region of maximum instability as assessed from the dry Richardson number condition is shown hatched. The cross-band wind profile is taken from the sounding nearest to the band, but not in the band, in order to minimize the influence of the band itself. Note that positive u is defined as toward the warm air.

The five bands studied are all moving at speeds corresponding to cross-band winds in the mid-troposphere (between 3 and 5 km height). None of the bands, however, are moving with the cross-band wind in the region of maximum instability. The disagreement is not serious. The altitude where the two speeds match is within a kilometer of the unstable region. It is also evident from the figures that there is substantial shear of the cross-band wind within the unstable layer. Shears of 2 to 5 m/s per km are observed in this layer. While such shear magnitudes are much less than the band-parallel shears in these regions (13-21 m/s per km), they are not negligible. The present linear theoretical model does not include a basic-state cross-band wind that varies with height. The observations suggest that this may be an important addition to the theory.

It should be emphasized that the observed winds used in the above analyses are assumed to be representative of the basic state. Recall that it is a cross-band circulation that is associated with the onset of symmetric instability. It is thus possible that some of the observed cross-band

wind speed may be due to the band perturbation in which case the above comparison of wind speeds is not meaningful.

3.4 The geostrophy of the observed wind shear.

In all of the previous assessments of the symmetric stability of the atmosphere it was assumed that the observed winds were representative of the geostrophically-balanced basic state. In particular, in the Richardson number analyses, it was assumed that the observed band-parallel wind shear is equal to the geostrophic shear. This assumption can be justified only if the band is oriented in the direction of the geostrophic shear and if the shear parallel to the band is equal in magnitude to the geostrophic shear.

It was shown in Fig. 7 that the band orientation tends to be close to the geostrophic shear direction. Even if these two directions differ by fifteen degrees, the magnitude of the band-parallel wind shear will differ by only 4% from the geostrophic wind shear as a result of choosing the wrong direction. Therefore the cross-band temperature gradient can be used to estimate the magnitude of the geostrophic shear. For each band case, two soundings on opposite sides of the band were used to estimate the temperature gradient between the two stations. The magnitude of the geostrophic wind shear is, from the thermal wind relation,

$$\frac{\partial V_g}{\partial z} \cong \frac{g}{f\bar{\theta}} \frac{\Delta\theta}{\Delta x} ,$$

where Δx is the distance between the two stations and $\Delta\theta$ is the potential temperature difference evaluated at any given height.

For five cases where the necessary soundings were available, vertical profiles were plotted of the estimated geostrophic wind shears and also of the band-parallel shears. The band-parallel wind shear is determined from the sounding nearest to the band. This is the same sounding that is used in the single sounding Richardson number analysis.

From comparison of the profiles it was found that in many regions of the atmosphere, the two shear magnitudes were markedly different. Table 5 lists the average band-parallel wind shear in the region of maximum instability and the estimated geostrophic wind shear in this region. The agreement is not good. In all five cases, the observed wind shear is supergeostrophic in the region of maximum instability. These discrepencies prompted a reassessment of the symmetric stability of the atmosphere substituting the geostrophic wind shear for the observed. The Richardson number condition of equation 1.3 was used for this reassessment. This can be written in terms of the horizontal temperature gradient as

$$Ri = \frac{f^2 \bar{\theta} \frac{\partial \theta}{\partial z}}{g \left(\frac{\partial \theta}{\partial x}\right)^2} < 1 ,$$

Table 5.

Case	Average Band Parallel Wind Shear (m/s/km)	Average Estimated Geostrophic Wind Shear (m/s/km)
12/05/81	12.5	6.5
12/11/82	9.0[1]	4.0[1]
12/20/82	12.4	6.8
01/11/83	11.3	8.7
01/11/84	12.2	5.4

[1] Value computed at level of maximum wind shear All other values are computed in the region of maximum instability.

Note: There is no region of maximum instability for the case 12/11/82.

or equivalently as

$$\frac{\partial \theta}{\partial x} > f\left[\frac{\theta_o}{g}\frac{\partial \theta}{\partial z}\right]^{\frac{1}{2}} . \qquad (3.4)$$

The quantity on the right-hand side of 3.4 is therefore the critical value of the temperature gradient for instability. If the observed temperature gradient is greater than this critical gradient, perturbations from the geostrophic basic state are theoretically unstable.

Vertical profiles of the critical temperature gradient were constructed for each case. The static stability $\partial\theta/\partial z$ was calculated using the nearest sounding to the band. Figures 13 a-e show these profiles computed for moist and dry adiabatic ascent and descent along with the observed cross-band temperature gradient estimated as described above.

In each case there are regions that are convectively unstable. In these regions the critical temperature gradient can be computed only for dry conditions. The region of maximum instability as previously assessed from a single sounding is indicated on each figure.

The regions previously assessed as unstable to dry symmetric overturning are now assessed as stable. Indeed, there are no regions of dry symmetric instability indicated for any of the five cases. Saturated conditions, in general, weaken the stability but except in the convectively unstable regions, the atmosphere is found to be stable or at

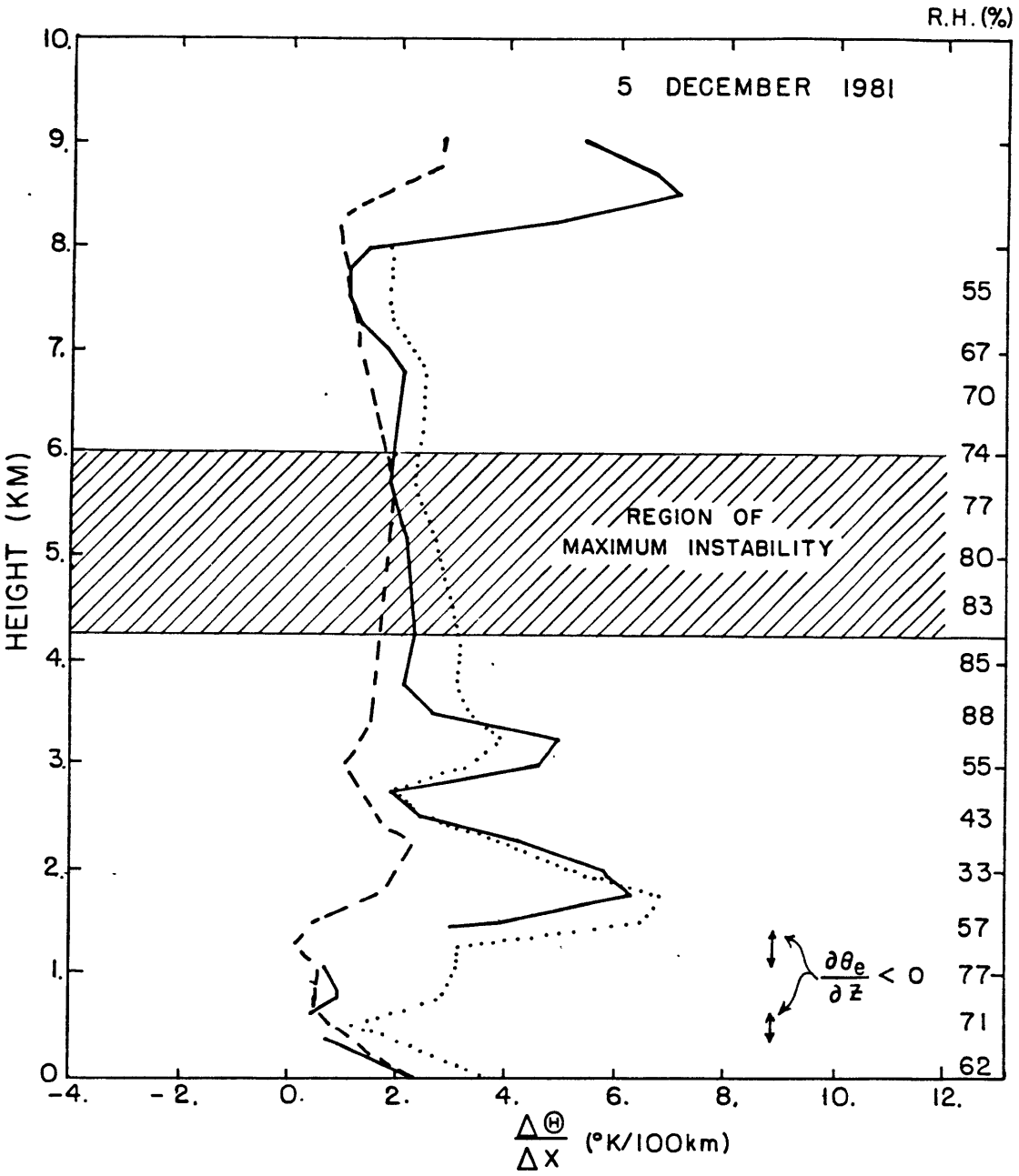

Fig. 13 a-e. Cross-band temperature gradient (°K/100km) as a function of height (km) for (a) 12GMT, 5 December 1981, (b) 12GMT 11 December 1982, (c) 12GMT, 20 December 1982, (d) 12GMT 11 January 1983, (e) 00GMT, 11 January 1984. Observed temperature gradient (dashed), critical temperature gradient for dry ascent (dotted), critical temperature gradient for moist ascent (solid).

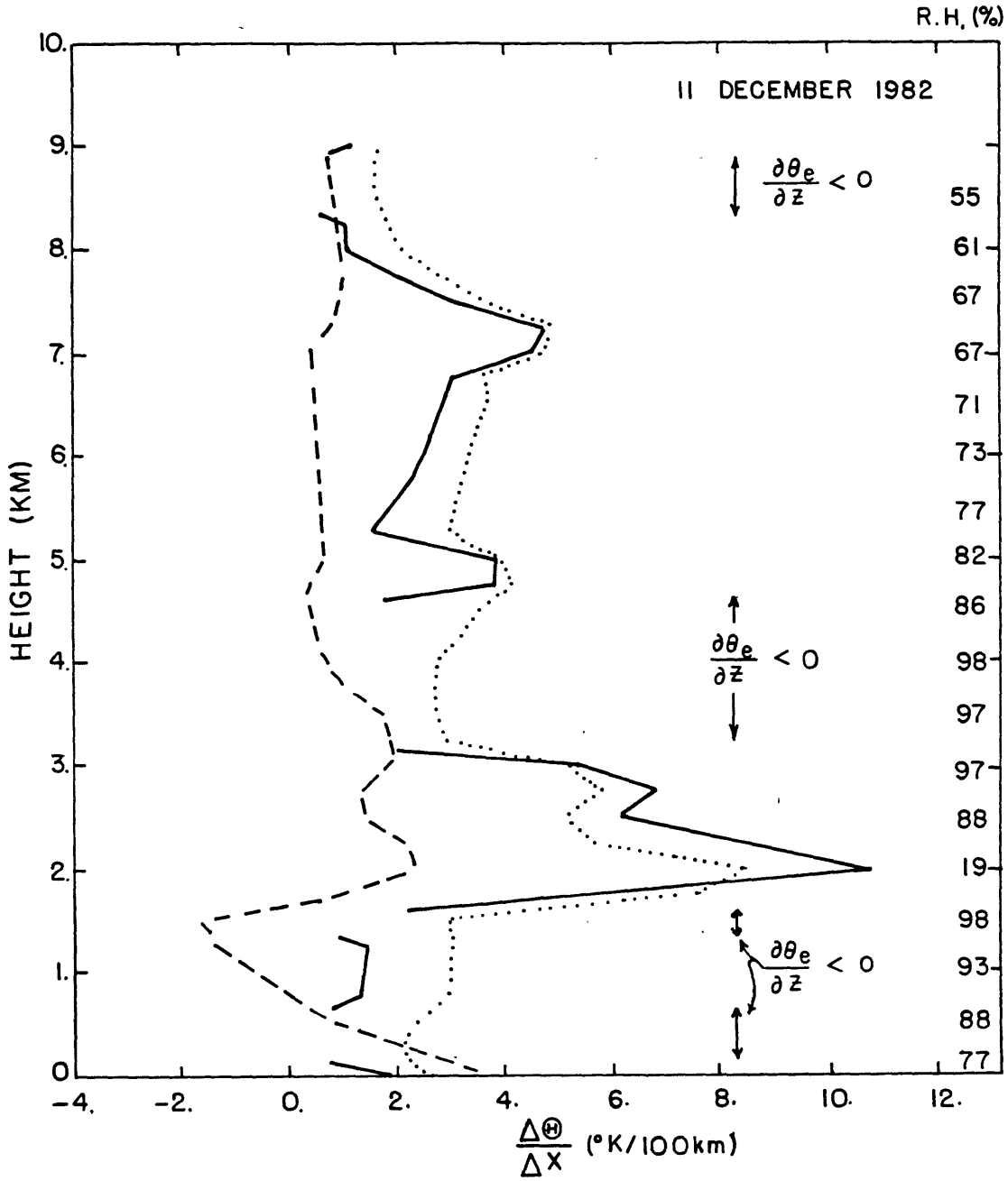
R.H. (%)
11 DECEMBER 1982
$\frac{\partial \theta_e}{\partial z} < 0$
$\frac{\partial \theta_e}{\partial z} < 0$
$\frac{\partial \theta_e}{\partial z} < 0$
HEIGHT (KM)
10.
9.
8.
7.
6.
5.
4.
3.
2.
1.
0
55
61
67
67
71
73
77
82
86
98
97
97
88
19
98
93
88
77
-4.
-2.
0.
2.
4.
6.
8.
10.
12.
$\frac{\Delta \Theta}{\Delta X}$ (°K/100km)

Fig. 13b

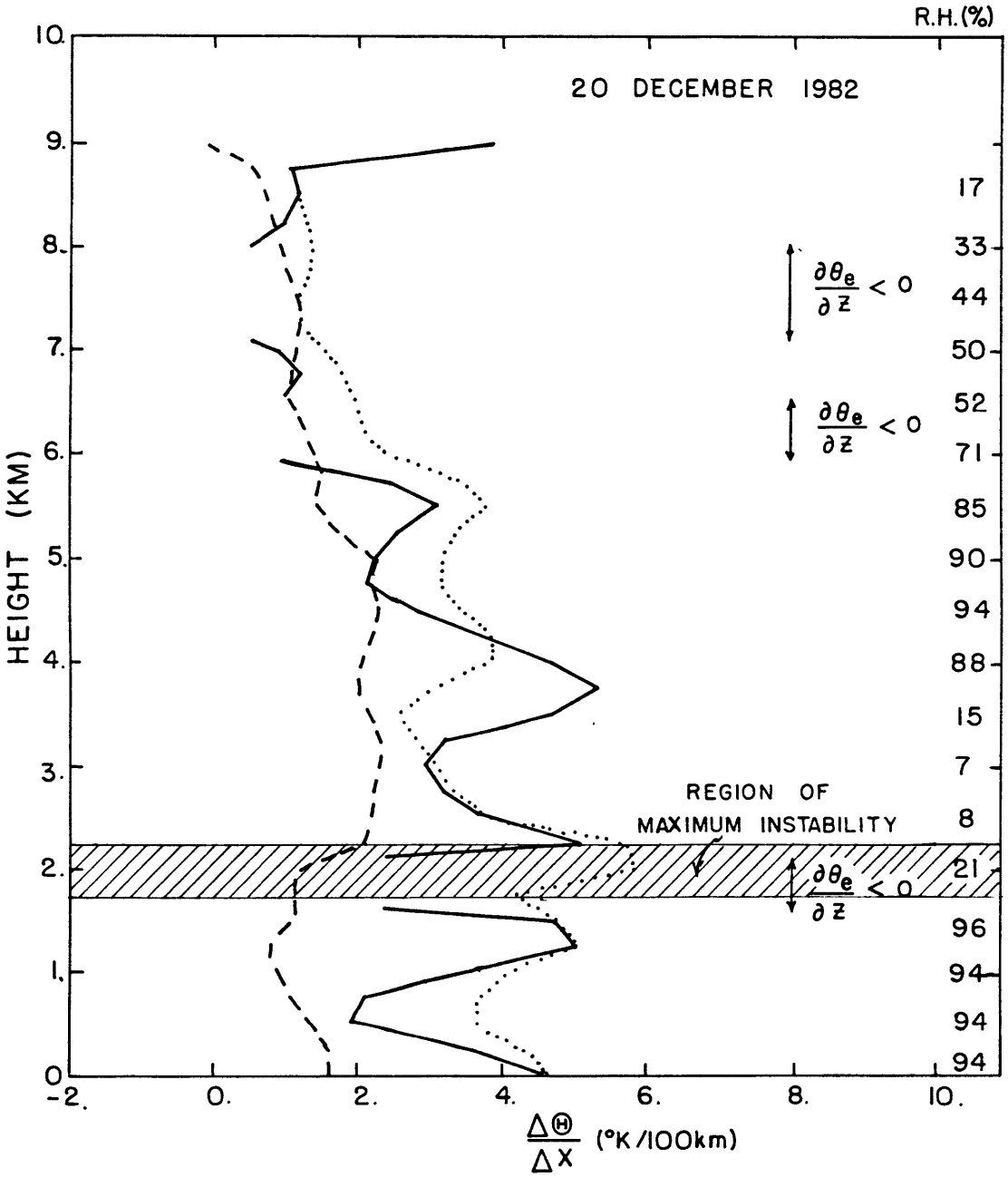
R.H.(%)
20 DECEMBER 1982
HEIGHT (KM)
10.
9.
8.
7.
6.
5.
4.
3.
2.
1.
0
-2.
0.
2.
4.
6.
8.
10.
17
33
44
50
52
71
85
90
94
88
15
7
8
21
96
94
94
94
$\frac{\partial \theta_e}{\partial z} < 0$
$\frac{\partial \theta_e}{\partial z} < 0$
REGION OF
MAXIMUM INSTABILITY
$\frac{\partial \theta_e}{\partial z} < 0$
$\frac{\Delta \Theta}{\Delta X}$ (°K/100km)

Fig. 13c

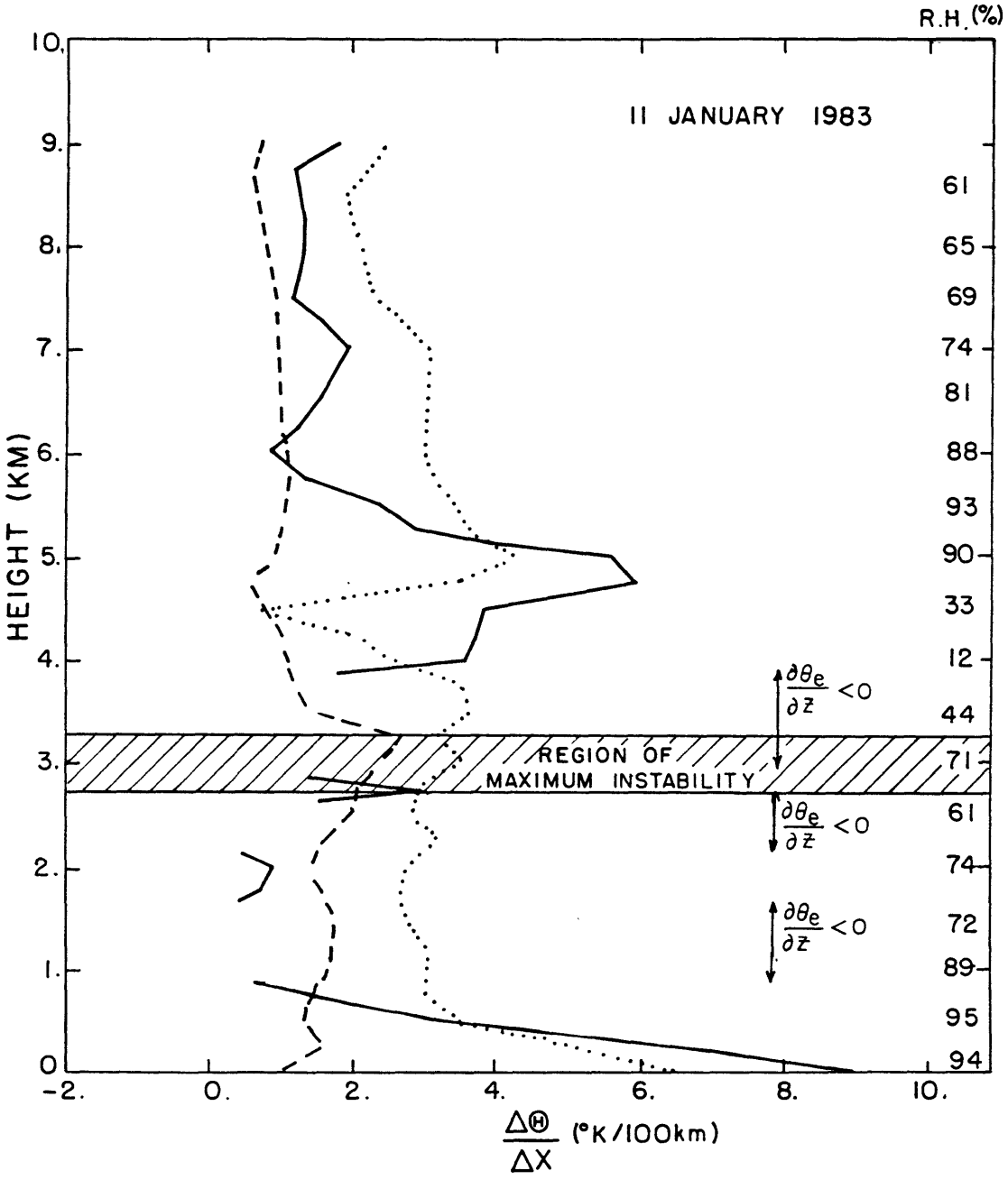
R.H.(%)
11 JANUARY 1983
HEIGHT (KM)
10.
9.
8.
7.
6.
5.
4.
3.
2.
1.
0
61
65
69
74
81
88
93
90
33
12
44
71
61
74
72
89
95
94
$\frac{\partial \theta_e}{\partial z} < 0$
REGION OF MAXIMUM INSTABILITY
$\frac{\partial \theta_e}{\partial z} < 0$
$\frac{\partial \theta_e}{\partial z} < 0$
-2.
0.
2.
4.
6.
8.
10.
$\frac{\Delta \Theta}{\Delta X}$ (°K/100km)

Fig. 13d

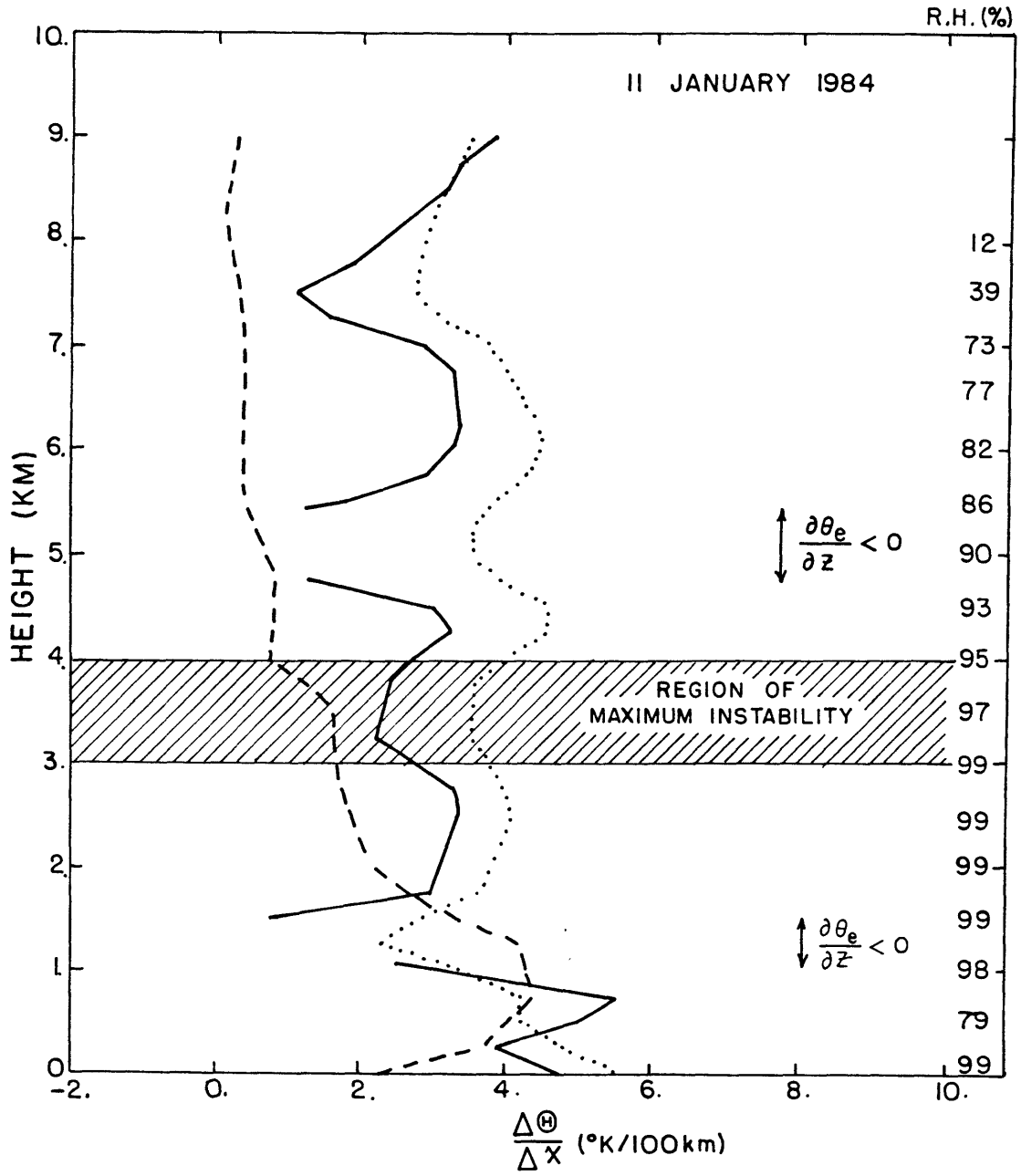
R.H. (%)
11 JANUARY 1984
HEIGHT (KM)
10.
9.
8.
7.
6.
5.
4.
3.
2.
1.
0
12
39
73
77
82
86
90
93
95
97
99
99
99
99
98
79
99
$\frac{\partial \theta_e}{\partial z} < 0$
REGION OF MAXIMUM INSTABILITY
$\frac{\partial \theta_e}{\partial z} < 0$
-2.
0.
2.
4.
6.
8.
10.
$\frac{\Delta \Theta}{\Delta x}$ (°K/100km)

Fig. 13e

most neutral to moist symmetric overturning. While the estimate in measuring the observed temperature gradient can be in error by as much as 1°C/100km, it is noteworthy that the estimate obtained never exceeds the critical value. It may be that the atmosphere is so efficient in restoring itself to a stable geostrophic balance that the theoretical instability condition can rarely be observed. However, such a possibility appears entirely inconsistent with the observed persistence of these bands.

Conclusions and suggestions for future work

This study was undertaken to examine the possible role of symmetric instability in the formation of precipitation bands. Observations from fifteen cases of banded and non-banded precipipation were used for this purpose.

The research completed to date is not sufficient to conclude whether or not symmetric instability is responsible for banded precipitation observed in the storms considered in this study. The banded observations do agree with certain aspects of the present linear theory.

The bands are embedded in regions of strong shear and are aligned close to the direction of the thermal wind. In nine of the eleven band cases, the band orientation was within 15 degrees of both the 1000-500 mb shear direction and the actual shear direction at the level of maximum instability. Observations provide evidence that the bands are quasi-two-dimensional with most of the horizontal variations in thermodynamic and kinematic properties occurring in the cross-band direction. Finally, the spacing between bands does agree with the predictions of the linear theory. Narrow regions of strong band-parallel shear in the middle troposphere, typically having magnitudes of ten to twenty m/s per km are observed to accompany the occurrence of banded precipitation. Substantial shears of five to ten m/s per km over very deep layers in the atmosphere are also observed when bands occur.

The two stability analyses used in this study depend on a knowledge of the direction and magnitude of the geostrophic wind shear. In assessing the symmetric instability of the atmosphere for each case, the observed band-parallel wind shear as measured from single soundings was assumed to represent the geostrophic basic state. It was shown that, insofar as choosing the direction is concerned, the band-parallel direction is a good approximation to the geostrophic shear direction. A much weaker assumption is that the band-parallel wind shear is close in magnitude to the geostrophic wind shear. These two assumptions lead to the conclusion that regions of the atmosphere for each band case are symmetrically unstable.

Indications of symmetric instability, however, were in most cases due to the strong shear regions in the middle troposphere that were confined to layers approximately one kilometer in depth. It was noted that symmetric instability is an imbalance that can arise in a geostrophically balanced atmosphere. It is unlikely that such a narrow region of strong shear can correspond to a geostrophic base state, for in that event, small-scale horizontal temperature gradients of a magnitude rarely observed in the atmosphere would have to exist in this region. When such gradients are observed, they are usually associated with ageostrophic, time-dependent circulations (e.g. mid-level frontogenesis) and not with a balanced flow.

In section 3, estimates were made of the geostrophic wind shear magnitude in five band cases to see how well they compare with the observed band-parallel wind shear. It was found that the agreement was poor in many parts of the soundings. It was shown that in the regions of the atmosphere assessed as symmetrically unstable (using the Richardson number analysis), the observed wind shear is highly ageostrophic. When the geostrophic shear magnitude was used to assess the symmetric stability for the five cases, indications were that most of the troposphere is symmetrically stable to infinitesimal perturbations under dry conditions. When the stability is assessed for moist adiabatic ascent, it is found that regions where the atmosphere is not convectively unstable are at most neutral to symmetric overturning.

Unfortunately, the measurement of the geostrophic basic state in these five studies was only an estimate. The poor spatial and temporal resolution of the sounding data used in this study may not be adequate to determine base state conditions. There are several ways to try to overcome this problem. Single and dual Doppler radar can be used to better determine the basic state wind field surrounding the band. To better represent thermodynamic as well as kinematic features, an instrumented airplane can be used to make passes through the band at various altitudes. Another solution would be to set up a dropsonde network in the

vicinity of the band. Simultaneous soundings could then be made with much better spatial and temporal resolution than the standard synoptic scale sounding network.

The estimates that were made of the geostrophic component of the observed wind shear in this study suggest either that the basic state in which bands form is not in geostrophic balance, or that the geostrophic basic state is not easily observed. The observations that the ageostrophic and geostrophic components of the shear are of comparable magnitude suggest that using a linearized model to examine the stability characteristics of a geostrophic basic state is not appropriate. It cannot be assumed that perturbations from the geostrophic basic state are small.

It has also been pointed out that the present theory does not explain the propagation of the band relative to the mean flow. The observations suggest that a basic state which includes a cross-band wind speed that varies with height may be required in the theoretical models.

Linking symmetric instability with banded precipitation can have major consequences. Operationally, the prediction of when and where bands will form and in what direction they will move is vital to producing a mesoscale forecast. Furthermore, such an instability may have important effects on the large scale flow. Stone (1972) and Emanuel (1984) have both suggested that symmetric instabi-

lity can result in appreciable transports of heat and momentum. If symmetric instability is responsible for the observed bands that occur so often in extratropical cyclones, the resulting heat and momentum transports should be more closely studied. A parameterization for such transports may be necessary in the current large-scale numerical models.

Acknowledgements

I am grateful to my advisor Prof. Richard Passarelli for his helpful suggestions, ideas, and support during this research. I thank Stephen Garner for the many hours of discussion we had concerning this thesis. Special thanks go to Spiros Geotis and Pauline Austin for their meticulous review of this thesis and to Isabelle Kole for her expedient drafting of the figures.

REFERENCES

Bennetts, D.A., and B.S. Hoskins, 1979: Conditional symmetric instability - a possible explanation for frontal rainbands. Quart.J.Roy.Meteor.Soc., 105, 945-962.

Bennetts, D.A., and J.C. Sharp, 1982: The relevance of conditional symmetric instability to the prediction of mesoscale frontal rainbands. Quart.J.Roy.Meteor.Soc., 108, 595-602.

Browning, K.A., and T.W. Harrold, 1969: Air motion and precipitation growth in a wave depression. Quart.J. Roy.Meteor.Soc. 95, 288-309.

Eliassen, A., 1962: On the vertical circulation in frontal zones. Geofys.Publ., Bjerknes Memorial Vol, 147-160.

Elliott, R.D., and E.L. Hovind, 1964: On convective bands within Pacific Coast storms and their relation to storm structure, J.Appl.Met., 3, 143-154.

Emanuel, K.A., 1979: Inertial instability and mesoscale convective systems. Part I. Linear theory of inertial instability. J.Atmos.Sci., 36, 2425-2449.

Emanuel, K.A., 1983: On assessing local conditional symmetric instability from atmospheric soundings. Mon. Wea.Rev., 111, (in press).

Emanuel, K.A., 1984: The Lagrangian parcel dynamics of moist symmetric instablity. J.Atmos.Sci., 40, 2368-2376.

Hoskins, B.J., 1974: The role of potential vorticity in symmetric stability and instability. Quart.J.Roy. Meteor.Soc., 100, 480-482

Houze, R.A., et al. 1976: Mesoscale rainbands in extratropical cyclones. Mon.Wea.Rev., 104, 868-878.

Ooyama, K., 1966: On the stability of baroclinic circular vortex: A sufficient criteria for instability. J.Atmos.Sci., 23, 43-53.

Parsons, D.B., and P.V. Hobbs, 1983: The mesoscale and and microscale structure and organization of clouds and precipitation in midlatitude cyclones. XI: Comparisons between observational and theoretical aspects of rainbands. J.Atmos.Sci., 40, 2377-2397.

Solberg, H., 1936: Le mouvement d'inertie de l'atmosphere stable et son role dans la theorie des cyclones. Memoir presented to the Meteor. Ass. of the U.G.G.I., Lisbon, Dupont Press, Paris.

Stone, P.H., 1966: On non-geostrophic baroclinic stability. J.Atmos.Sci., 23, 310-400.

Stone, P.H., 1972: On non-geostrophic baroclinic stability: Part III. The momentum and heat transports. J.Atmos. Sci., 29, 419-426.